



AGR-1, AGR-2, AGR-3/4, and AGR-5/6/7 Dimensional- Change Analysis

July 2023

John Merickel and Binh Pham



*INL is a U.S. Department of Energy National Laboratory
operated by Battelle Energy Alliance, LLC*

DISCLAIMER

This information was prepared as an account of work sponsored by an agency of the U.S. Government. Neither the U.S. Government nor any agency thereof, nor any of their employees, makes any warranty, expressed or implied, or assumes any legal liability or responsibility for the accuracy, completeness, or usefulness, of any information, apparatus, product, or process disclosed, or represents that its use would not infringe privately owned rights. References herein to any specific commercial product, process, or service by trade name, trade mark, manufacturer, or otherwise, does not necessarily constitute or imply its endorsement, recommendation, or favoring by the U.S. Government or any agency thereof. The views and opinions of authors expressed herein do not necessarily state or reflect those of the U.S. Government or any agency thereof.

AGR-1, AGR-2, AGR-3/4, and AGR-5/6/7 Dimensional- Change Analysis

John Merickel and Binh Pham

July 2023

**Idaho National Laboratory
Advanced Reactor Technologies
Idaho Falls, Idaho 83415**

<http://www.art.inl.gov>

**Prepared for the
U.S. Department of Energy
Office of Nuclear Energy
Under DOE Idaho Operations Office
Contract DE-AC07-05ID14517**

Page intentionally left blank

INL ART Program

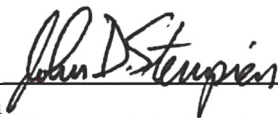
**AGR-1, AGR-2, AGR-3/4 and AGR-5/6/7 Dimensional
Change Data Analysis**

INL/RPT-16-37916

Revision 1

July 2023

Technical Reviewer:

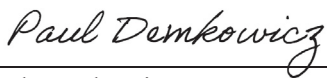


John Stempien
Technical Reviewer

7/11/2023

Date

Approved by:



Paul Demkowicz
AGR Program Technical Director

7/11/2023

Date



Travis Mitchell
INL ART Program Manager

6/26/2023

Date



Michelle T. Sharp
INL Quality Assurance

6/26/2023

Date

Page intentionally left blank

ABSTRACT

A series of Advanced Gas Reactor (AGR) experiments has been completed in the Advanced Test Reactor at Idaho National Laboratory in support of qualification and development of tristructural isotropic fuel. Each AGR test consists of multiple independently controlled and monitored capsules containing fuel compacts placed in a graphite cylinder. These capsules are instrumented with thermocouples embedded in the graphite, enabling temperature control. Fuel compacts are composed of fuel particles surrounded by a graphitic A3 matrix material. Knowledge about the dimensional change in AGR fuel compacts during irradiation is important because the swelling or shrinkage affects the size of the gas gaps that are used to control temperature. Analysis of dimensional change in the AGR fuel compacts is performed to establish a functional relationship with the variables directly relating to compact dimensional changes and support the refinement of thermal calculations that model the sizes of the gaps between components in the irradiation experiment.

The variables initially identified for consideration were matrix density, compact density, fuel packing fraction, fuel-particle diameter, cumulative fast-neutron fluence, fluence rate, matrix grade and time average volume average fuel temperature. In addition to the data from the AGR experiments, the analysis included specimens formed from the same A3 matrix material used in Advanced Graphite Creep (AGC) experiments, which provide graphite-creep data during irradiation for design and licensing purposes. The primary purpose of including the AGC specimens was to compare with the dimensional changes of AGR compacts.

All possible combinations of first-order variable regressions were considered in the analysis. The study focused on identifying the best regression models for percent change in diameter, length, and volume. Linear model diagnostics were used to ensure the resulting regression models were robust and performed well. The variables identified as very significant in predicting change in one or more dimensions (diameter, length, and volume) are volume average time average temperature, fast fluence, matrix density, packing fraction, and fuel-particle diameter. Due to the presence of confounding effects between several variables, interpretation of these results is equivocal; the use of multiple statistical tests provides additional confidence in the conclusion.

Page intentionally left blank

CONTENTS

ABSTRACT.....	iii
ACRONYMS.....	ix
1. INTRODUCTION.....	1
2. EXPERIMENTAL DESIGN	2
3. DIMENSIONAL CHANGES	5
3.1. Compact Diameter	5
3.2. Compact Length.....	6
3.3. Compact Volume	7
4. DIMENSIONAL CHANGE STATISTICAL ANALYSIS	9
4.1. Compact Dimension Explanatory Variables.....	10
4.2. Model Specification and Estimation	12
5. RESULTS	13
5.1. Change in Compact Diameter.....	13
5.1.1. Fitting data from individual experiments.....	14
5.1.2. Fitting data from all experiments	14
5.1.3. Investigate influence of the compact matrix-graphite grade.....	17
5.1.4. Investigate influence of the fluence rate	18
5.1.5. Comparison of model with only fluence vs. full model.....	21
5.2. Change in Compact Length.....	21
5.2.1. Fitting data from individual AGR experiments	22
5.2.2. Fitting data from all AGR experiments.....	22
5.2.3. Investigating influence of the compact-matrix graphite grade.....	24
5.2.4. Investigating influence of the fluence rate	25
5.3. Change in Compact Volume	27
5.3.1. Fitting data from individual AGR experiments	27
5.3.2. Fitting data from all AGR experiments.....	28
5.3.3. Investigate influence of the compact matrix graphite grade	30
5.3.4. Investigate influence of the fluence rate	30
6. DISCUSSION	32
6.1. Different Dimension Change Behavior for Individual AGR Experiments	33
6.2. Dimensional Change for all AGR Experiments.....	35
7. CONCLUSION	40
8. REFERENCES.....	41

FIGURES

Figure 1. AGR-1 test train axial schematic (left) and radial cross section of a capsule (right).	2
Figure 2. AGR-3/4 axial schematic (left) and radial cut of a capsule (right).....	3
Figure 3. Cross sections of the AGR-5/6/7 capsules, showing the compact stacks.....	4
Figure 4. AGC-2 graphite compacts axial schematic (top) and radial cross section of a capsule (bottom).	4
Figure 5. Box plots for FAB and PIE compact diameters by AGR experiment.	5
Figure 6. Box plots for FAB and PIE compact lengths by experiment.....	7
Figure 7. Box plots for FAB and PIE compact volume by experiment.	8
Figure 8. Effect plots of model fit to all AGR data for percent change in compact diameter.	16
Figure 9. Observed versus predicted percent change in diameter.....	17
Figure 10. Effect plot of a two level categorical variable for matrix grade.	18
Figure 11. Interaction plot of effective full power days and fluence.	19
Figure 12. Plot of continuous fluence rate effect for model of percent change in compact diameter.	20
Figure 13. Observed vs. predicted plot for model predicting compact diameter percent change as function of fluence.....	21
Figure 14. Effects plots for variables selected for the model of percent change in compact length.....	23
Figure 15. Plot of observed versus predicted values for percent change in compact length for AGR experiments.	24
Figure 16. Effect plot of matrix grade on percent change in compact length.	25
Figure 17. Interaction effect plot for effective full power days with fluence on percent change in compact length.....	26
Figure 18. Effect plot for fluence rate on diameter percent change.....	27
Figure 19. Effects plot for selected model of percent change in compact volume.	29
Figure 20. Observed versus predicted percent change in compact volume for model fit.	29
Figure 21. Effect plot of matrix grade for model fit to volume percent change.	30
Figure 22. Effect plot for the interaction of EFPD with fluence to predict percent change in volume.	31
Figure 23. Effect plot of fluence rate as continuous predictor of percent volume change.....	32
Figure 24. Percent change in diameter as a function of fluence and TAVA temperature by experiment.	34
Figure 25. Percent change in length as a function of fluence and TAVA temperature by experiment.	34
Figure 26. Percent change in volume as a function of fluence and TAVA temperature by experiment.	35
Figure 27. Percent change in diameter of all compacts as a function of fluence.	37

Figure 28. Percent change in length of all compacts as a function of fluence.	38
Figure 29. Percent change in volume of all compacts as a function of fluence.	39

TABLES

Table 1. Summary statistics for measured FAB and PIE compact diameters in mm included in this analysis by experiment.	6
Table 2. Summary statistics for measured FAB and PIE compact lengths in mm, based on the compacts included in this analysis.	6
Table 3. Summary statistics for calculated FAB and PIE compact volume in <i>mm</i> ³ across experiments included in this analysis.	8
Table 4. Summary statistics for explanatory variables utilized in the analysis across experiments.	10
Table 5. Variables selected from LASSO regression applied to each experiment individually.	14
Table 6. Linear regression model parameter estimates and ANOVA table for fit to all AGR data for percent change in compact diameter.	15
Table 7. ANOVA table from model fit including a categorical predictor for graphite grade used in the matrix material for model of percent diameter change.	17
Table 8. ANOVA table of full model showing an interaction effect of effective full power days and cumulative fluence for percent change in diameter.	19
Table 9. ANOVA table for full model with continuous effect of fluence rate added for modeling percent change in compact diameter.	20
Table 10. Selected variables for linear models for percent change in compact length for each AGR experiment.	22
Table 11. ANOVA table and parameter estimates from selected model for AGR data for compact length.	22
Table 12. ANOVA table for percent change in length with a factor for matrix grade incorporated.	24
Table 13. ANOVA of model for percent change in length with incorporation of effective full power days and an interaction effect to test for a fluence rate effect.	25
Table 14. ANOVA for percent change in length with added effect of fluence rate.	26
Table 15. Variables selected for models of volume percent change fit to each experiment separately.	28
Table 16. ANOVA table and coefficient estimates for selected model fit to all AGR experiments for percent volume change.	28
Table 17. ANOVA table of model fit with categorical predictor for matrix grade.	30
Table 18. ANOVA table showing the main effect of EFPD and an interaction effect of EFPD with fluence.	31
Table 19. ANOVA table resulting from fit of model including continuous effect of fluence rate on percent volume change.	32
Table 20. Regression coefficients for percent change in diameter, length, and volume models.	35

Page intentionally left blank

ACRONYMS

AGC	Advanced Graphite Creep
AGR	Advanced Gas Reactor
AIC	Akaike Information Criteria
ANOVA	Analysis of variance
ART	Advanced Reactor Technologies
ATR	Advanced Test Reactor
EFPD	Effective full-power day
FAB	Fabrication
HTGR	High temperature gas-cooled reactor
INL	Idaho National Laboratory
IPyC	Inner pyrolytic carbon
LASSO	Least Absolute Shrinkage and Selection Operator
NEFT	Northeast flux trap
OPyC	Outer pyrolytic carbon
PIE	Post-irradiation examination
TA	Time average
TAVA	Time average volume average
TRISO	Tristructural isotropic

Page intentionally left blank

AGR-1, AGR-2, AGR-3/4, and AGR-5/6/7 Dimensional-Change Analysis

1. INTRODUCTION

A series of fuel-irradiation experiments have been conducted in the Advanced Test Reactor (ATR) at Idaho National Laboratory (INL) to support the licensing and operation of the Advanced Reactor Technologies (ART) high-temperature gas-cooled reactor (HTGR). The Advanced Gas Reactor (AGR) Fuel Development and Qualification experiments consist of between five and twelve independent capsules containing multiple cylindrical fuel compacts, placed inside a graphite holder in the ATR. The AGR experiments provide data on fuel performance under irradiation and potential accident conditions, support fuel process development, qualify the fuel for normal operating conditions, provide irradiated fuel for potential accident testing, and support the development of fuel performance and fission-product transport models. All four AGR irradiation campaigns have been completed: AGR-1 (December 2006–November 2009); AGR-2 (June 2010–October 2013); AGR-3/4 (December 2011–April 2014); and AGR-5/6/7 (February 2018–July 2020).

Tristructural isotropic (TRISO) particles consist of a central spherical kernel composed of a heterogeneous mixture of uranium carbide and uranium oxide. These kernels were encased in a low-density carbon buffer, dense inner pyrolytic carbon (IPyC), silicon carbide (SiC), and dense outer pyrolytic carbon (OPyC) layers to form the particles (Petti et al. 2012). The SiC layer provides structural integrity and retains fission products at elevated temperatures during irradiation.

The fuel particles are then overcoated with resinated-graphite matrix precursor powder and pressed into right cylindrical compacts, with the matrix material filling in the spaces between the TRISO fuel spheres. The AGR-1, 2, and 3/4 compact matrix was formed from the German A3-3-style resinated graphite powder. The A3-3-style resinated graphite powder was produced using a 20:80 blend of synthetic and purified natural flake graphite powders by weight. The powders were resinated with a viscous, alcohol-soluble resol phenolic resin containing formaldehyde as a hardening agent. The shelf life of the resin was limited and required refrigeration to slow polymerization and crosslinking reactions. On the other hand, the resinated graphite powder for the AGR-5/6/7 experiment was similar to the German A3-27 formulation, but used a novolac phenolic resin flake, which was partially cross-linked instead of phenol. The novolac resin (Durite SD-1708) has no integral hardening agent and a much longer shelf life than a resol resin. The graphite blend was a 20:80 blend of synthetic (SGL KRB2000) and purified natural flake (Asbury 3482) graphite (Marshall 2020).

Irradiation-induced dimensional changes in AGR fuel compacts are important because the swelling or shrinkage affects the size of the gas gaps that are used in thermal models to calculate fuel temperatures. The goal of analyzing dimensional changes in the AGR fuel compacts is to establish significant factors impacting compact shrinkage, including exposure to fast neutrons.

In parallel, a series of graphite irradiation experiments have been conducted at ATR to support the design of graphite core components for HTGRs. The Advanced Graphite Creep (AGC) experiments use matched pairs of stressed and unstressed graphite specimens to assess the effects of irradiation on dimensional and thermomechanical properties. Seventeen AGC-2 pure-graphite specimens were included for comparison. These AGC-2 specimens were selected because they were machined from a similar A3 graphite matrix material that was used in the AGR fuel-compact matrix, and they were not subjected to mechanical stress during irradiation. For the sake of simplicity, the word compact will be used to collectively refer to both the AGR fuel compacts and the AGC specimens throughout this report.

2. EXPERIMENTAL DESIGN

For all experimental test trains, the capsule components are given unique identifiers and cataloged to preserve the identity of the component and the location within the test train from which the component was removed. For example, the capsule number, level within the capsule, and stack number were recorded for each compact. Each experimental test train had a different setup, which is illustrated in Figure 1 through Figure 4.

The AGR-1 test train was a multicapsule, instrumented lead experiment, designed for irradiation in the 38.1-mm-diameter B-10 (large B) position of the ATR. The test train contained six capsules, each independently controlled for temperature and independently monitored for fission-product-gas release. An axial view of the test train is illustrated in Figure 1 (left). Each AGR-1 capsule was 152.4 mm long and contained 12 fuel compacts arranged in three vertical stacks with four compacts each. Figure 1 (right) displays a radial cross section of a capsule illustrating the arrangement of the three compact stacks and showing the hafnium (Hf) shroud used to suppress the thermal-neutron flux on the west side of the capsule (Collin 2015).

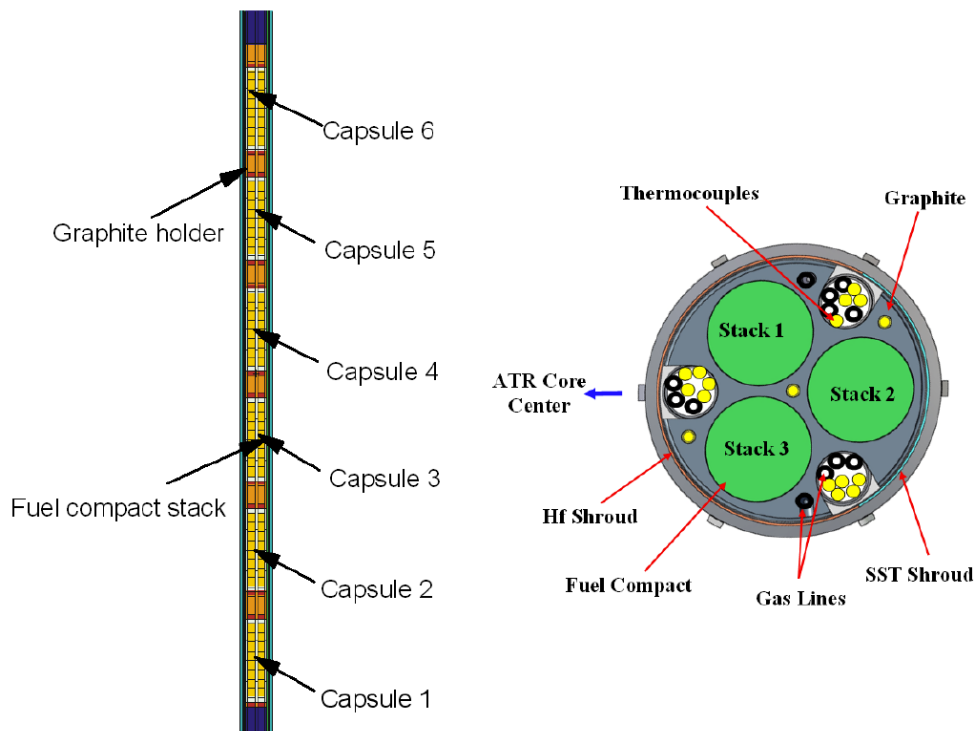


Figure 1. AGR-1 test train axial schematic (left) and radial cross section of a capsule (right).

The AGR-2 test train was nearly identical to the AGR-1 test train but was designed for irradiation in the 38.1-mm-diameter B-12 (large B) position of the ATR. Five of the six AGR-2 capsules were 152.4 mm long and contain 12 fuel compacts arranged in three vertical stacks of four compacts. The compacts in AGR-2 Capsule 1 were different in dimension from the other AGR-2 compacts and are not included in this analysis (Collin 2014).

The AGR-3/4 experiment was placed in the northeast flux trap (NEFT) position in the ATR core. An axial view of the irradiation test train and two of the 12 capsules is shown in the side of Figure 2 (left). Four through tubes carried thermocouples and gas lines to each individual capsule. All 12 capsules had their own gas supply and return line. Figure 2 (left) also represents the arrangement of capsules stacked together to form the experiment train. Each capsule has a stack of four fuel compacts in the center surrounded by three annuli of graphite and/or graphitic matrix material, as shown in the radial cut of the capsule in Figure 2 (right). While 48 compacts in 12 capsules were used in the AGR-3/4 experiment, 24 compacts from six fuel-body capsules were unable to be measured during PIE because compacts were retained in the graphite rings. Therefore, only 24 compacts were measured during PIE and used in this analysis (Collin 2016).

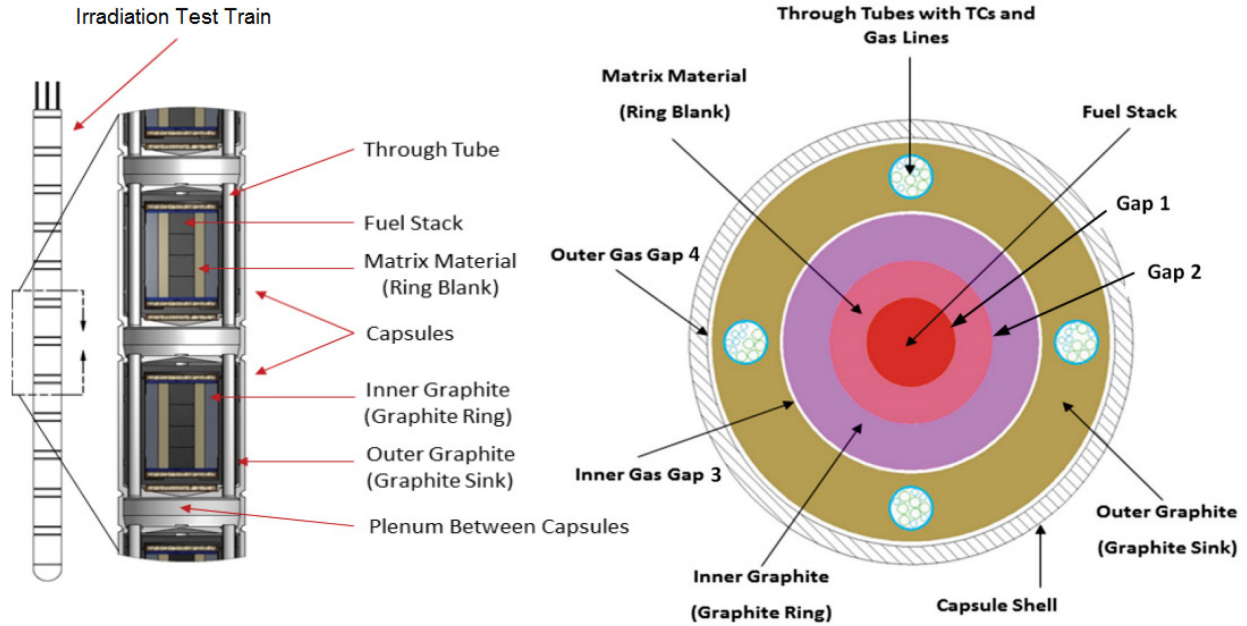


Figure 2. AGR-3/4 axial schematic (left) and radial cut of a capsule (right).

AGR-5/6/7 was the last in the series of AGR experiments, irradiated in the NEFT position of the ATR core from February 2018 to July 2020 (Pham et al. 2021). Five capsules containing 194 fuel compacts comprised AGR-5/6/7. Fuel compacts in each capsule were housed in several stacks within a graphite holder (Figure 3). Capsule 1 had ten fuel stacks with nine compacts per stack; Capsule 2 had four compacts with eight compacts per stack, Capsules 4 and 5 had four stacks with six compacts per stack; and Capsule 3 had three stacks, with eight compacts per stack, arranged in an inner graphite holder. Diameter and length data for 193 of the 194 AGR-5/6/7 compacts measured during the PIE were included in this analysis because Compact 2-8-4 was broken during disassembly and could not be measured (Stempien and Cai 2023).

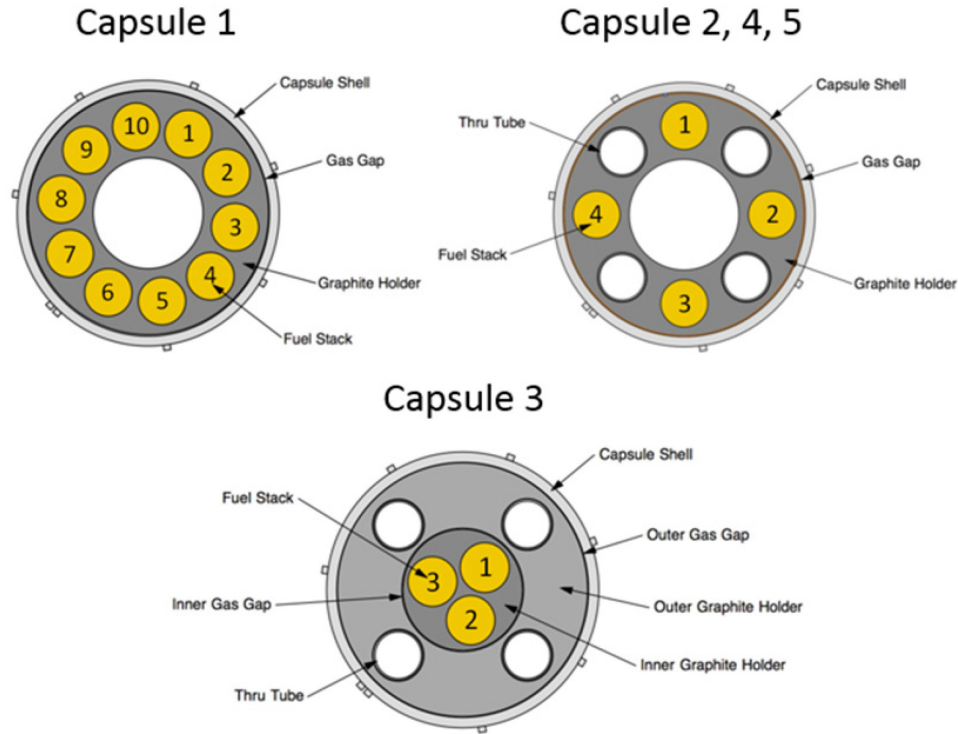


Figure 3. Cross-sections of the AGR-5/6/7 capsules, showing the compact stacks.

The unfueled AGC-2 experiment consisted of one fully instrumented capsule irradiated in the south flux trap of ATR. The capsule contained a specimen holder with six equally spaced channels around a single central channel (Figure 4). Each irradiation capsule was composed of over 400 graphite specimens that were characterized before and after irradiation to determine the irradiation-induced material-property changes and life-limiting irradiation creep rate for each graphite grade. AGC graphite compacts used in this analysis were in the center channel or bottom half of the outer channels and did not receive any mechanical stress. These blank compacts were composed of A3 graphitic matrix material, which is the same material as the fuel-compact matrix of the AGR experiments (Windes et al. 2015).

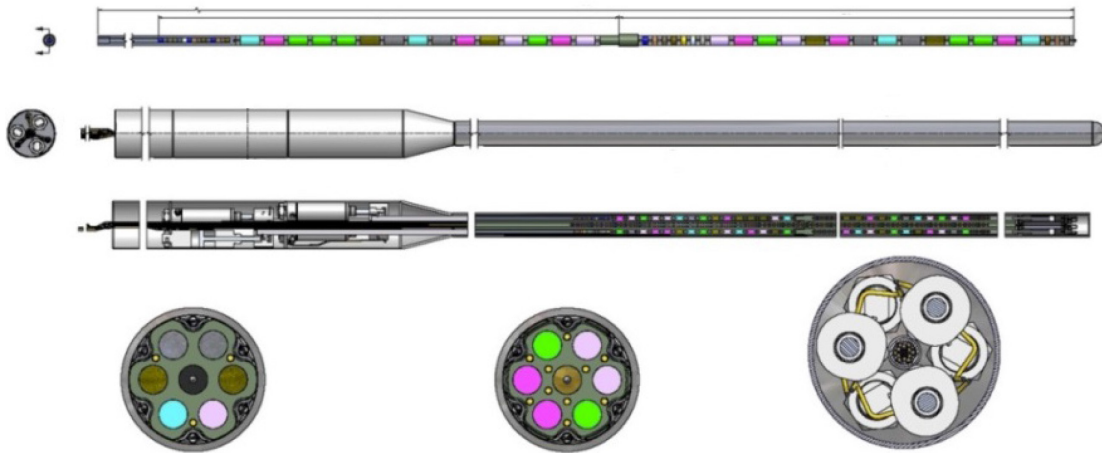


Figure 4. AGC-2 graphite compacts axial schematic (top) and radial cross-section of a capsule (bottom).

3. DIMENSIONAL CHANGES

Dimensional data for the AGR fuel compacts and AGC graphite compacts (length, diameter, and volume) were analyzed to determine whether significant changes were seen between the as-fabricated (FAB) and PIE measurements. All data utilized in this analysis originated from the Nuclear Data Management and Analysis System 2.0 database (Hull 2012).

3.1. Compact Diameter

AGR compact diameters varied within a small range, from 11.97 to 12.37 mm. Summary statistics of FAB and PIE compact diameters are given in Table 1. Figure 5 shows boxplots by experiment for FAB and PIE diameter. For each category, the mean value is depicted by a “+” symbol in the boxplot. The median is the middle line in the boxplot, with the 25th and 75th percentiles indicated at the ends of each box. The whiskers denote the minimum and maximum and encompass the range of the data. Note that each FAB boxplot is much smaller in range than the respective PIE boxplot.

Diameters are measured multiple times per compact at different axial regions for both FAB and PIE; the number of replications was dependent on the experiment. Results from a paired t-test indicate there is a statistically significant difference between FAB and PIE diameters for all experiments with the PIE diameters consistently smaller than the FAB diameters (Figure 5).

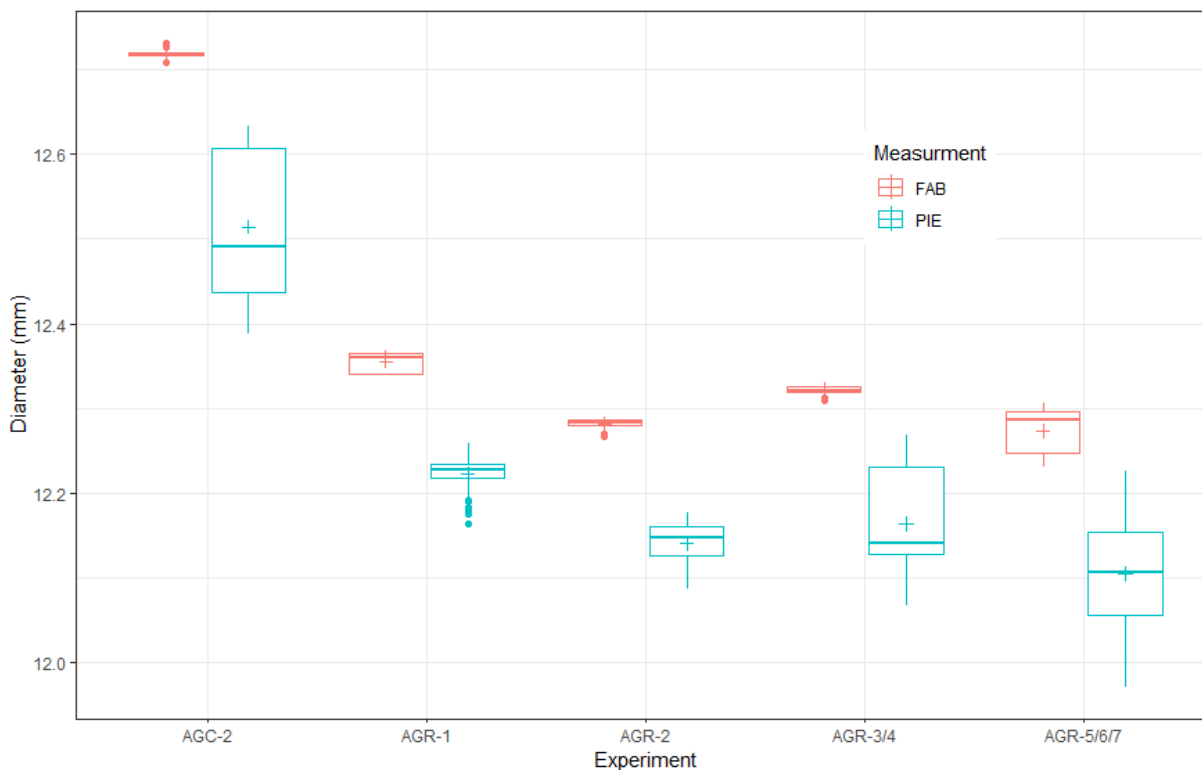


Figure 5. Box plots for FAB and PIE compact diameters by AGR experiment.

Table 1. Summary statistics for measured FAB and PIE compact diameters in millimeters included in this analysis by experiment.

Experiment	Measurement	Number of Compacts	Average (mm)	Standard Deviation (mm)	Average % Change
AGC-2	FAB	17	12.72	0.01	-1.65
AGC-2	PIE	17	12.51	0.09	
AGR-1	FAB	72	12.36	0.01	-1.13
AGR-1	PIE	72	12.22	0.02	
AGR-2	FAB	48	12.28	0.01	-1.14
AGR-2	PIE	48	12.14	0.02	
AGR-3/4	FAB	24	12.32	0.01	-1.30
AGR-3/4	PIE	24	12.16	0.06	
AGR-5/6/7	FAB	193	12.27	0.03	-1.30
AGR-5/6/7	PIE	193	12.11	0.06	

3.2. Compact Length

The FAB and PIE compact lengths ranged from 6.25 to 25.45 mm, and their summary statistics are presented in Table 2. Measurement methods for FAB and PIE length differ. AGR FAB compact lengths represent a single measurement using a micrometer probe placed at the center of one end of the compact (Demkowicz et al. 2011). AGC FAB length was measured at various positions with a micrometer (Windes et al. 2014). AGR-1 and AGR-2 PIE lengths were measured using a machine vision system, with measurements taken at three orientations (Demkowicz et al. 2011, Ploger et al. 2015). PIE lengths for AGR-3/4 compacts were measured with a micrometer; only one measurement was taken on each compact (Stempien et al. 2016). AGR-5/6/7 compact length also was measured only once per compact (Stempien and Cai 2023). AGC PIE lengths were measured at various positions with a Vernier caliper (Windes et al. 2015).

Table 2. Summary statistics for measured FAB and PIE compact lengths in mm, based on the compacts included in this analysis.

Experiment	Measurement	Number of Compacts	Average (mm)	Standard Deviation (mm)	Average % Change
AGC-2	FAB	17	6.32	0.01	-0.47
AGC-2	PIE	17	6.29	0.05	
AGR-1	FAB	72	25.12	0.09	-0.64
AGR-1	PIE	72	24.96	0.09	
AGR-2	FAB	48	25.14	0.02	-0.56
AGR-2	PIE	48	25	0.05	
AGR-3/4	FAB	24	12.51	0.02	-0.40
AGR-3/4	PIE	24	12.46	0.04	
AGR-5/6/7	FAB	193	24.91	0.2	-0.52
AGR-5/6/7	PIE	193	24.78	0.24	

Figure 6 shows a panel of boxplots of the FAB and PIE length by experiment. Multiple plots are presented because the length of the AGR-3/4 compacts are half the length of the rest of the AGR compacts, and the blank AGC-2 compacts are half the length of the AGR-3/4 compacts. Therefore, different scales on the y-axes are needed. Initial observations of the boxplots of FAB and PIE compact length indicate length was on average less for PIE than FAB. However, the whiskers on the boxplots show that the PIE length was more variable than the FAB lengths and particularly variable for the AGR-5/6/7 compacts.

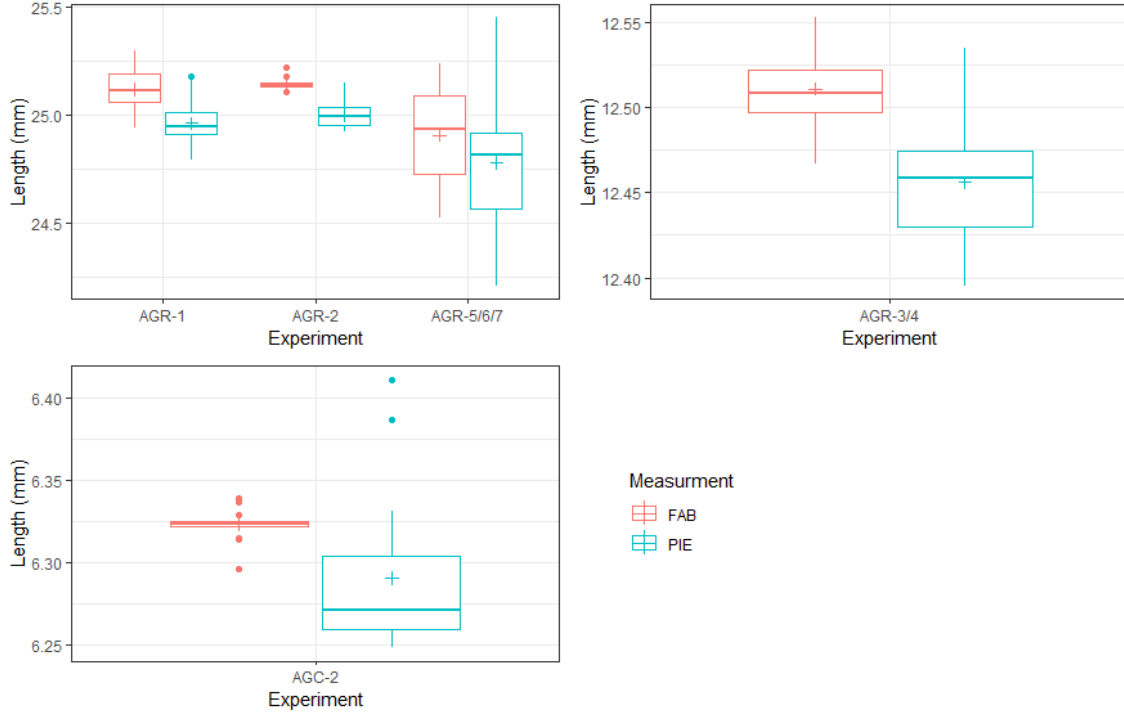


Figure 6. Box plots for FAB and PIE compact lengths by experiment.

3.3. Compact Volume

Compact volumes for FAB and PIE were calculated from length and diameter, using the equation for the volume of a cylinder as seen in Equation (1).

$$\text{Volume of a Cylinder} = \pi * \left(\frac{1}{2} \text{diameter}\right)^2 * \text{length} \quad (1)$$

Calculated volume for a compact ranged from 762.05 to 3025.56 mm³. Due to this large range, boxplots are provided separately for three different volume ranges, as shown in Figure 7. As expected, the smaller PIE compact lengths and diameters lead to smaller PIE volumes for most compacts when compared to the FAB values, except for some AGR-5/6/7 compacts that had numerous PIE lengths longer than the FAB length (Figure 6). The summary of compact volume by experiment in Table 3 also shows the PIE volumes are mostly smaller than FAB volumes for AGR and AGC-2 compacts.

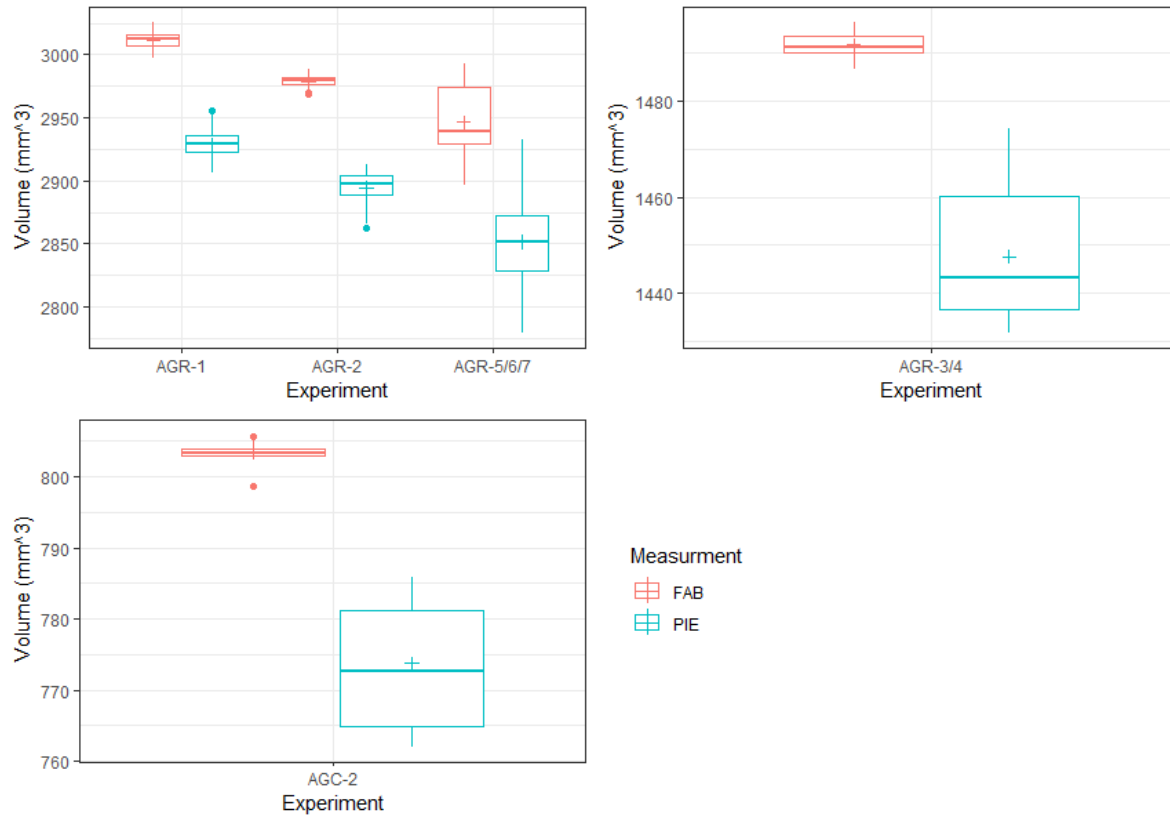


Figure 7. Box plots for FAB and PIE compact volume by experiment.

Table 3. Summary statistics for calculated FAB and PIE compact volume in cubic millimeters across experiments included in this analysis.

Experiment	Measurement	Number of Compacts	Average (mm³)	Standard Deviation (mm³)	Average % Change
AGC-2	FAB	17	803.4	1.5	-3.70
AGC-2	PIE	17	773.7	8.3	
AGR-1	FAB	72	3011.6	6.1	-2.74
AGR-1	PIE	72	2929	10.4	
AGR-2	FAB	48	2978.5	4.4	-2.83
AGR-2	PIE	48	2894.2	13.7	
AGR-3/4	FAB	24	1491.8	2.4	-2.96
AGR-3/4	PIE	24	1447.6	13.8	
AGR-5/6/7	FAB	193	2946.5	24.8	-3.22
AGR-5/6/7	PIE	193	2851.5	32.1	

4. DIMENSIONAL CHANGE STATISTICAL ANALYSIS

The objective of the analysis is to develop a statistical model that adequately explains variation in compact dimensional change and allows for inference on factors that are related to the dimensional change in compacts. In 2016, an analysis of dimensional-change data was conducted using data from AGC-2, AGR-1, AGR-2, and AGR-3/4. Here, we expand on that analysis by including AGR-5/6/7 data, and we use a refined variable selection and modeling approach to help better understand factors related to dimensional change of compacts.

Changes in compact dimensions are important because of the impact on gas gaps used in thermal models to calculate fuel temperatures, which are important factors in assessing performance of fuel irradiated in the AGR experiments. More compacts were irradiated in AGR and AGC capsules than the number of compacts used in this analysis due to measurement constraints during PIE. Among AGR compacts, 18 compacts from AGR-2 Capsules 1 and 4 were excluded due to significant size differences and to protect proprietary data, and dimensions of 24 compacts embedded in the six AGR-3/4 fuel-body capsules could not be measured during PIE. As a result, 337 out of a total of 380 fuel compacts from the four AGR experiments were used in the analysis, based on the available PIE dimensional data.

Each capsule differs in composition and irradiation exposure; because of the many groups that needed to be compared, there is a high risk of confounding of effects with differences among the groups. For example, there may be a difference in compact dimensional change as a function of graphite grade, but because all AGR-5/6/7 compacts were made with A3-27 graphite while all AGR-3/4 compacts were made with A3-3 graphite, the effect of graphite grade could be a confounding of irradiation conditions between the two experiments, for example. To mitigate the effects of such confounding, we will attempt to control for irradiation conditions such as irradiation temperature and fluence as well as important manufacturing differences when assessing the effects of variables. To summarize, we want to assess the effects of one variable among compacts that are comparable in both irradiation conditions and manufacturing properties to ensure we can make strong inferences on factors affecting dimensional change.

The percent of dimensional change was chosen as the response variable because it is unitless and allows measurements for different experiments to be compared. The time-averaged (TA) minimum, TA maximum, and time-averaged volume-averaged (TAVA) temperatures are highly correlated so only one of them will be selected for use in models. Compact density and matrix density are also correlated ($\rho \approx 0.9$), and one of the two variables must be selected over the other. Choosing the most appropriate variable for temperature and matrix vs compact density is done using goodness of fit metrics like R^2 .

In the previous version of this analysis, fluence squared was included in modeling as it was found to be a good predictor of dimensional change; however, here we only focused on first-order main effects. This focus decreases model complexity and allows for straightforward interpretations of factors affecting dimensional change. The only interaction of main effects considered here is that of EFPDs and fluence to investigate a possible effect of fluence rate. This, however, can also be assessed with a continuous main effect of fluence divided by EFPDs as a proxy for fluence rate.

4.1. Compact Dimension Explanatory Variables

The primary variables related to conditions in the experimental test trains that have been well documented to effect dimensional change of graphite (i.e., fuel compacts using a graphite matrix) include end-of-irradiation cumulative fast-neutron fluence (n/m^2 , $E > 0.18 \text{ MeV}$) and time-averaged volume-averaged temperature (TAVA) per compact (Demkowicz 2011). The effects of additional variables are also investigated. The following independent variables and their data sources are included in this analysis:

1. TA Minimum, TA maximum, and TAVA temperatures per compact for AGR-1, 2, 3/4, and 5/6/7 were taken from these reports (Hawkes, 2014, 2014b, 2016, 2021), respectively.
2. Fast fluence data for AGR-1,-2, 3/4, and 5/6/7 were taken from these reports (Sterbenz 2013, 2014, 2015, 2020), respectively.
3. Fluence rate (effectively a TA neutron flux) on the change in compact dimension by incorporating the effects of EFPDs for each of the four AGR experiments.
4. Matrix grade: AGR-1, 2, and 3/4 experiments used grade A3-3 graphitic matrix and AGR-5/6/7 used grade A3-27.
5. Independent variables associated with compact manufacturing include matrix density, compact density, particle packing fraction and particle diameter. The fuel properties data were taken for AGR-1 from these reports (Hull et al. 2006s); for AGR-2 from these reports: (Hull et al. 2010s); for AGR-3/4 from these reports: (Hull et al. 2007, 2011 and Hull 2011); and for AGR-5/6/7 from (Marshall 2019).

It is important to note that these independent variable values may have changed from previous versions of this document due to changes in thermal-model calculations and other changes; however, the most up-to-date values are used in this analysis. Specifically, the particle diameters used in this analysis are slightly different from those given in the first-look PIE reports (Demkowicz et al. 2011, Floger et al. 2015, Stempien and Cai 2023). In the absence of particle-diameter measurements (i.e., for AGR-5/6/7), available kernel diameter and thicknesses of three outer layers were used to calculate the particle diameter. For consistency, the same calculated particle diameter was used for all experiments. Therefore, particle diameters in Table 4 are slightly different from the actual as-fabricated particle diameters measured for a subset of particles. Summary statistics for the independent variables across all experiments are recorded in Table 4.

Table 4. Summary statistics for explanatory variables used in the analysis across experiments.

Variable	Unit	Mean	Standard Deviation	Minimum	Maximum
Experiment = AGR-1 (72 compacts)					
Particle Diameter	μm	786.97	1.4	785.11	789.11
Packing Fraction	ratio	0.366	0.005	0.36	0.374
Matrix Density	g/cm^3	1.293	0.045	1.219	1.344
TAVA Temperature	$^{\circ}\text{C}$	1044	40	955	1136
TA Minimum Temperature	$^{\circ}\text{C}$	903	55	800	1044
TA Maximum Temperature	$^{\circ}\text{C}$	1138	32	1069	1197
Fast Fluence/ 10^{24} ($E > 0.18 \text{ MeV}$)	n/m^2	3.502	0.567	2.167	4.298
Compact Density	g/cm^3	1.818	0.033	1.766	1.881
EFPD	days	620.0	—	—	—

Variable	Unit	Mean	Standard Deviation	Minimum	Maximum
Experiment = AGR-2 (48 Compacts)					
Packing Fraction = 0.23 (12 UO ₂ compacts)					
Particle Diameter	μm	953.09	0.00	953.09	953.09
Packing Fraction	ratio	0.23	0	0.23	0.23
Matrix Density	g/cm ³	1.68	0.01	1.67	1.69
TAVA Temperature	°C	1032	27	996	1062
TA Minimum Temperature	°C	945	49	889	999
TA Maximum Temperature	°C	1090	12	1072	1105
Fast Fluence/10 ²⁴ (E > 0.18 MeV)	n/m ²	3.35	0.20	3.05	3.53
Compact Density	g/cm ³	2.05	0.00	2.05	2.07
EFPD	days	559.2	—	—	—
Packing Fraction = 0.37 (36 UCO compacts)					
Particle Diameter	μm	862.47	0.00	862.47	862.47
Packing Fraction	ratio	0.37	0	0.37	0.37
Matrix Density	g/cm ³	1.59	0.01	1.58	1.61
TAVA Temperature	°C	1142	87	987	1296
TA Minimum Temperature	°C	1021	91	868	1199
TA Maximum Temperature	°C	1224	87	1080	1360
Fast Fluence/10 ²⁴ (E > 0.18 MeV)	n/m ²	2.94	0.45	1.94	3.47
Compact Density	g/cm ³	2.11	0.00	2.11	2.12
EFPD	days	559.2	—	—	—
Experiment = AGR-3/4 (24 compacts)					
Particle Diameter	μm	808.4	0	808.4	808.4
Packing Fraction	ratio	0.362	0.001	0.361	0.364
Matrix Density	g/cm ³	1.598	0.005	1.59	1.608
TAVA Temperature	°C	1114	175	832	1376
TA Minimum Temperature	°C	1055	165	790	1335
TA Maximum Temperature	°C	1162	186	865	1418
Fast Fluence/10 ²⁴ (E > 0.18 MeV)	n/m ²	3.628	1.527	1.195	5.286
Compact Density	g/cm ³	2.01	0.003	2.004	2.017
EFPD	days	369.2	-	NA	NA
Experiment = AGR-5/6/7 (193 compacts)					
Nominal Packing Fraction = 0.25 (79 compacts)					
Particle Diameter	μm	847.35	0.00	847.35	847.35
Packing Fraction	ratio	0.253	0.003	0.0248	0.0256
Matrix Density	g/cm ³	1.77	0.01	1.75	1.78
TAVA Temperature	°C	968	220	736	1338
TA Minimum Temperature	°C	841	235	536	1249

Variable	Unit	Mean	Standard Deviation	Minimum	Maximum
TA Maximum Temperature	°C	1045	222	843	1405
Fast Fluence/ 10^{24} ($E > 0.18$ MeV)	n/m ²	5.02	0.42	4.00	5.55
Compact Density	g/cm ³	2.10	0.01	2.08	2.11
EFPD	days	360.9	—	—	—
Nominal Packing Fraction = 0.40 (114 compacts)					
Particle Diameter	μm	847.35	0.00	847.35	847.35
Packing Fraction	ratio	0.384	0.001	0.382	0.387
Matrix Density	g/cm ³	1.75	0.01	1.73	1.76
TAVA Temperature	°C	933	138	621	1097
TA Minimum Temperature	°C	756	131	458	898
TA Maximum Temperature	°C	1043	150	726	1210
Fast Fluence/ 10^{24} ($E > 0.18$ MeV)	n/m ²	3.05	0.84	1.62	4.40
Compact Density	g/cm ³	2.26	0.01	2.24	2.27
EFPD	days	360.9	—	—	—

4.2. Model Specification and Estimation

To provide useful models with logical inference, we used linear models fit with maximum likelihood and least squares. Though some effects may be nonlinear in nature, we are interested primarily in making inferences on factors causing dimensional change (not prediction), and without differential equations available to define relationships among variables, linear approximations are most useful to interpret. Modeling assumptions of normally distributed, homoscedastic residuals with zero mean will be assessed to make sure the assumptions of linear regression are met, and that a linear approximation is indeed appropriate.

We are primarily interested in developing an inferential model; however, we still want to avoid over-parameterization to ensure we can make sensible inferences that can be appropriately generalized to other datasets. We selected variables to include in the models by using significance testing in conjunction with information criteria and goodness of fit metrics to achieve a balance between goodness of fit and model complexity (parsimony). To determine the most-appropriate variables for inclusion in the model, multiple statistical tests were considered. The models created are expressed as:

$$Y = B_1X_1 + B_2X_2 + B_3X_3 + B_4X_4 + B_5X_1X_2 \quad (2)$$

Here $B_1 - B_5$ are the explanatory variable coefficients and X_1, X_2, X_3 , and X_4 are the observed variable values and the last term X_1X_2 represents an interaction effect of the variables X_1 and X_2 . The Y represents the percent change in the dimensional variable we are trying to describe, or the dependent variable. Notice there is no β_0 intercept term in this linear model; this is because the previous version of this analysis found the intercept was not beneficial, and we feel the assumption of no change in dimensions at a zero value for the covariates is reasonable. The best-performing model, as determined by several statistical factors, was selected from a pool of several logical combinations of the explanatory variables described above. The regression models are based upon the range of the data available and should not be extrapolated beyond the range of the data provided.

The selection of variables used the most-logical variables known to influence dimensional change of fuel compacts; however, some additional models were used to investigate other hypotheses as well. One such hypothesis is that the grade of graphite used in the compact matrix may have an impact on dimensional changes due to irradiation; hence, a term for graphite grade was incorporated. The effect of fluence rate is investigated two ways: by incorporating an interaction term in the model for EFPDs and fluence and by incorporating a continuous effect into the full model for fluence rate by dividing fluence by EFPDs. By conditioning on the number of full-power days a compact was irradiated, we can compare dimensional change to other compacts that achieved similar cumulative fluences—but over shorter or longer periods—and assess whether fluence rate may be a factor important to dimensional change.

The statistical methods outlined above were implemented to identify variables that significantly impact dimensional change. SAS software version 9.4 (SAS, 2013) was used primarily for model fitting and variable selection and R (R, 2023) was used for data visualization. Sections 5.1–5.3 cover the statistical tests by dimension-response variables and basic output. The variables of dimensional change considered were compact diameter, length, and volume. For each dimension, the following analysis will be performed:

1. Fit models using each AGR dataset separately.
2. Fit models using all AGR data.
3. Investigate influence of the compact matrix graphite grade using all AGR data.
4. Investigate influence of the compact fluence rate.

5. RESULTS

Confounding of factors among experiments (AGC-2, AGR-1, AGR-2, AGR-3/4 and AGR-5/6/7 experiments) proved difficult to deal with when selecting variables that explained the most variation in dimensional change. Initial investigations suggested that the inherent differences between the AGR data and the AGC data were problematic for model estimation and hindered inference on variable effects across experiments. Therefore, the 17 AGC-2 compacts were excluded to mitigate confounding. Also, only the first order main effects were considered in the statistical models for fitting to the dimensional data from AGR experiments. This reduced confounding and allowed us to make inference on factors influencing dimensional change.

5.1. Change in Compact Diameter

The percent change in compact diameter was calculated as:

$$\text{percent change in Diameter} = \frac{PIE \text{ Diameter} - FAB \text{ Diameter}}{FAB \text{ Diameter}} * 100 \quad (3)$$

In this revised analysis, 18 compacts in two capsules containing non-US fuel were excluded from the AGR-2 experiment while 193 AGR-5/6/7 compacts were added to the data set for inclusion in the analysis, resulting in a total of 337 compacts. The Akaike information criteria (AIC) (Akaike 1974) in conjunction with least absolute shrinkage and selection operator (LASSO) regression (Tibshirani 1996) were used to select influential variables for inclusion in linear-regression models. The term variable selection is widely used in statistics, but often not explicitly defined. Here we use the term selected to specifically mean that the variables selected using LASSO regression and AIC are considered the most-important variables of the suite of potential variables for predicting percent change in compact dimensions, and inclusion of variables outside of those selected would not provide significant improvement in model fit to warrant their inclusion in the model.

Initially, several models were fitted using all three temperatures (i.e., TA minimum, TA maximum, and TAVA temperatures) to assess which temperature metric would be the most-important predictor. As a result, the TAVA temperature was the best predictor and from here on, the TAVA temperature is referred to as TAVA in the regression models. Next, models with TAVA and matrix density and with TAVA and compact density were compared using AIC and R-squared. The results showed that matrix density explained slightly more variation in dimensional change—or was more influential—than compact density. Therefore, TA minimum temperature, TA maximum temperature, and compact density are excluded from further analyses. The correlation between TAVA and fluence was also calculated because it would be expected that these be correlated with each other; however, we found that across all AGR experiments, fluence and TAVA were only ~30% correlated, which is well below our threshold of 90% correlation at which removal of a variable is necessary.

5.1.1. Fitting data from individual experiments

Confounding factors among experiments made variable selection difficult, so we initially applied LASSO regression to a subset of potential main effects, including TAVA, cumulative fluence, compact packing fraction, matrix density, and particle diameter, to each experiment separately. At this step in the analysis, we did not investigate effects of EFPDs or matrix grade because those variables have only one value for each experiment. The results of the variables selected for inclusion for each experiment are given in Table 5.

Table 5. Variables selected from LASSO regression applied to each experiment individually.

Experiment	Variables Selected
AGR-1	TAVA + Particle Diameter
AGR-2	TAVA + Fluence + Packing Fraction + Particle Diameter
AGR-3/4	TAVA + Fluence + Packing Fraction
AGR-5/6/7	TAVA + Fluence + Matrix Density

Table 5 shows that TAVA was selected as an important variable for every experiment, and cumulative fluence is selected in three out of the four experiments. This is consistent with the previous dimensional-change analyses and the literature on nuclear graphite behavior. It is interesting to note that packing fraction was also selected in three of four models while particle diameter was selected twice and matrix density only for the AGR-5/6/7 data. It is noteworthy that the model selected for AGR-1 did not include fluence, but rather TAVA and particle diameter, only. Figure 23 in the discussion section sheds light on this because there was very little variation in the AGR-1 percent change in diameter as a function of fluence. Particle diameter was also selected as an important variable for AGR-2 data, but not for the AGR-3/4 or AGR-5/6/7 data. This is because AGR-1 and AGR-2 had multiple particle diameters whereas AGR-3/4 and AGR-5/6/7 had only one particle diameter for all compacts. As in the previous dimensional-change analysis, the intercept term was excluded from linear models as it did not provide any improvement of fit to the models. Also, dimensional change should be zero when fluence is zero. Therefore, the intercept term from all the linear models was assumed to be zero.

5.1.2. Fitting data from all experiments

The LASSO regression-variable selection routine was applied to the complete data set from all the AGR experiments. A model with all five predictors was selected based on AIC from the LASSO regression. As expected, all five predictors in Table 5 are somewhat important. An analysis of variance (ANOVA) table is presented as Table 6 for the selected best-fit model for percent change in compact diameter for all AGR data, including the estimated regression coefficients (B_1 : B_5 as given in Equation (2) and corresponding sums of squares.

Table 6. Linear-regression model parameter estimates and ANOVA table for fit to all AGR data for percent change in compact diameter.

Variable	Estimate	Sum of Squares	Df	F-Value	P-Value
TAVA	-0.000567	1.95	1	52.531	2.99E-12
Fluence	-0.1822	7.267	1	195.816	2.20E-16
Packing Fraction	0.4202	0.145	1	3.903	0.04902
Matrix Density	-0.7508	3.149	1	84.853	2.20E-16
Particle Diameter	0.001245	1.187	1	31.985	3.36E-08

The second column in Table 6 gives the estimated regression coefficients from the fit and can be used to predict percent change in compact diameter with Equation (4). Similar equations can be derived from the estimated regression coefficients for the length and diameter percent change models presented later, but for brevity, we only write out the equation for the model of percent change in compact diameter.

$$\%Change\ in\ Diameter\ for\ Compact_i = -0.000567 * TAVA_i - 0.1822 * \left(\frac{Fluence_i}{10^{24}} \right) + \quad (4)$$

$$0.4202 * Packing\ Fraction_i - 0.7508 * Matrix\ Density + 0.001245 * Particle\ Diameter \quad (5)$$

The R-squared of the fit was 98%, indicating the selected model predicts percent diameter change well. The sums of squares column of Table 6 indicates the relative importance of the variables; cumulative fluence and matrix density stand out as explaining large portions of variance in the percent change of diameter (i.e., most-influential factors), followed by TAVA, particle diameter, and packing fraction. We can also see the p-value of packing fraction is nearly 0.05, indicating less support for it being a significant predictor. This is almost the same set of variables that was selected in the previous analysis of the data up to AGR-3/4, but matrix density was also found to be significant in this analysis when we included AGR-5/6/7 data. A slight difference between the previously selected model and the one selected here is the inclusion of fluence rather than fluence squared in this model. We did not consider fluence squared for a potential variable because initial investigations indicated a linear relationship of diameter change with fluence was sufficient. For convenience, the regression model presented above is referred to as the global model for percent change in compact diameter to differentiate from models that include the effects of matrix density or fluence rate. To better interpret the relationships of the selected variables with percent diameter change, it is useful to look at an effect plot (Figure 8) of the fitted model.

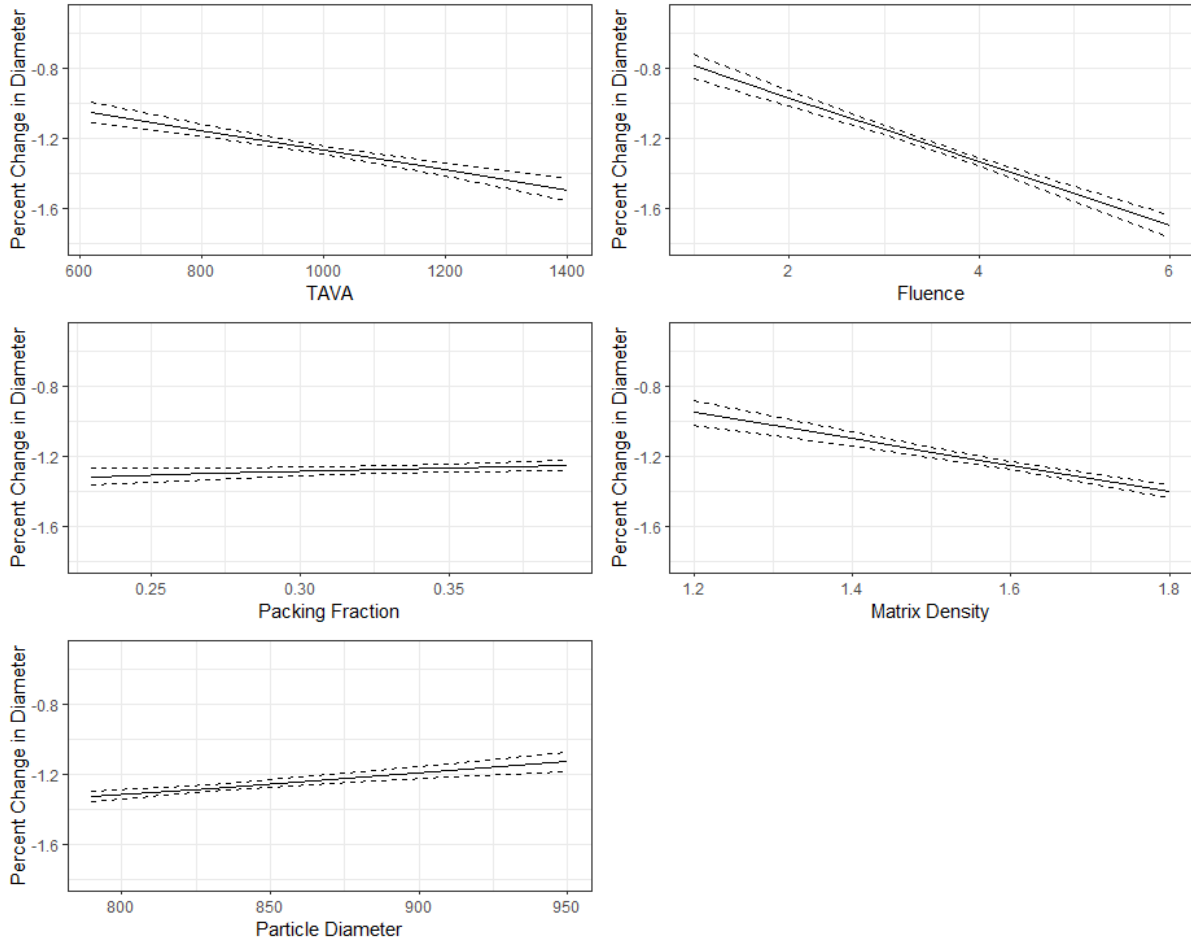


Figure 8. Effect plots of model fit to all AGR data for percent change in compact diameter. The solid lines represent the predicted value for percent change in diameter as a function of the variable labelled on each x-axis while the other four model variables are held at their mean value. The dashed lines represent 95% confidence limits.

Figure 8 shows the predicted values as a function of the estimated regression coefficients multiplied by their corresponding independent variable values while all other variables are held to their mean value. The plots of TAVA and fluence show, as we would expect, that compacts shrink more in diameter as TAVA and cumulative fluence increases. We also see that an increase in matrix density results in greater shrinkage in the diameter of compacts. Conversely, the plots of particle diameter and packing fraction indicate that, as they increase, compact diameters shrink less. It is important to note, however, that some of these relationships may be driven by confounding factors. AGR-5/6/7 had a very large sample size relative to the other experiments, and the matrix density of all the compacts in AGR-5/6/7 were between 1.73 and 1.78 g/cm³, so part of the matrix-density effect could be due to other, unaccounted for differences of AGR-5/6/7 from the other experiments, such as matrix-graphite grade.

To assess the overall fit of the selected model, the predicted values resulting from the model fit were plotted against their corresponding observed percent change in compact diameter (Figure 9). Additionally, we confirmed the assumptions of linear regression for normally distributed residuals with mean zero and homoscedastic variance were met with a histogram of the residuals and used to calculate a mean of the residuals to be 6.2E-5 (essentially zero). The observed-versus-predicted plot indicates no systematic bias in the model predictions, and the data from each experiment are evenly distributed on both sides of the 1:1 line indicating the model explains variation in the data from all experiments well.

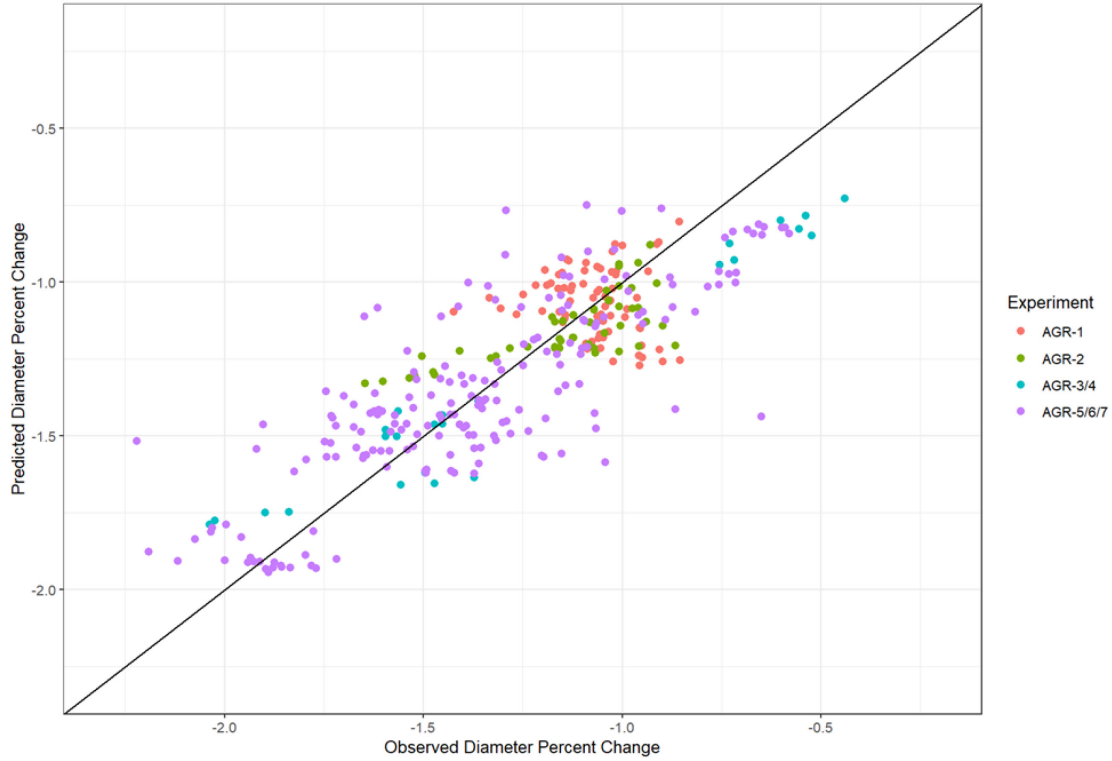


Figure 9. Observed versus predicted percent change in diameter. The black line indicates the 1:1 line, where all values would lie in the optimistic case of a perfect fit.

5.1.3. Investigate influence of the compact matrix-graphite grade

To further investigate other potential factors influencing percent change in diameter, we added a categorical variable to the model presented in Table 5 for matrix grade and subsequently refit the model. Table 7 shows the resulting estimated parameters and estimation information.

Table 7. ANOVA table from model fit, including a categorical predictor for graphite grade used in the matrix material for model of percent diameter change.

Variable	Sum Sq	Df	F-Value	P-Value
Mean TAVA Temp	1.9315	1	52.4487	3.134E-12
Fluence	3.6331	1	98.6539	2.2E-16
Packing Fraction	0.0842	1	2.2872	0.131406
Matrix Density	0.3156	1	8.569	0.003657
Particle Diameter	0.0496	1	1.346	0.246814
Matrix Grade	0.1686	2	2.2895	0.102919

According to the sums of squares column and P-value columns (Table 7), cumulative fluence and TAVA are still the most-influential independent variables, and both are highly significant (P-value much less than 0.05). But the packing fraction and particle diameter are not highly significant. The P-value for matrix grade indicates that there is some evidence of an effect here. However, this is highly confounded because all A3-27 grade graphite compacts are from the AGR-5/6/7 experiment. The estimated regression coefficients are not included in Table 7 to reduce clutter, but all the effects included in the first model remain unchanged in direction (estimates have same sign in Table 7 and Table 6) in the refit model. However, it is useful to plot the effect of matrix grade for better interpretation (Figure 10).

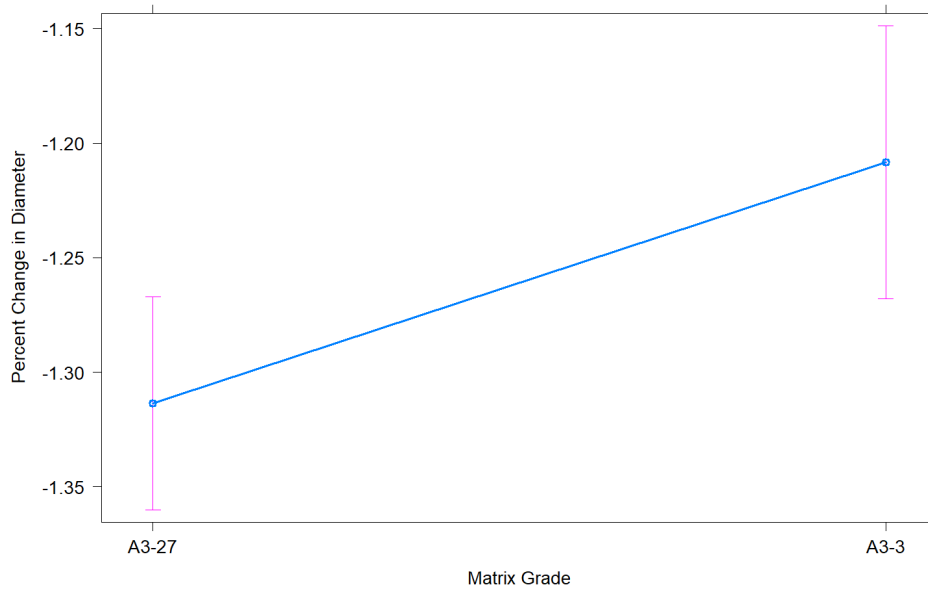


Figure 10. Effect plot of a two-level categorical variable for matrix grade. Pink error bars represent 95% confidence intervals.

We see a nearly significant difference (about 90% confident there is a difference) between the percent change in diameter of the two grades of graphite used in the matrix of the compacts (i.e., between the A3-3 vs. the A3-27 grade). In other words, on average the compacts with A3-27 grade matrix graphite shrunk by 1.31% while compacts with A3-3 grade graphite shrunk by an average 1.2% while holding all other variables to their mean values. We provide this caveat, though, because this is essentially just comparing the AGR-5/6/7 compacts' change in diameter to the other AGR experiments average change in diameter while controlling for the other variables in the model; therefore, other differences between the experiments could also be driving this effect.

5.1.4. Investigate influence of the fluence rate

To assess the possible effect of fluence rate, we incorporated a categorical main effect of EFPDs and an interaction effect of EFPDs and fluence. Table 8 gives the ANOVA table from the model fit with the interaction. The interaction term at the bottom of the Table 8 has a P-value of less than 0.05, indicating a significant effect of the interaction. The main effect of EFPDs is significant as well; however, because the interaction of EFPD and fluence is significant, the interpretation of the main effect is not straightforward. Thus, we focus on the interaction. Notice, in Table 8, that packing fraction, matrix density, and particle diameter are no longer significant. This indicates that the effect of fluence rate (interaction between fluence and EFPDs) is explaining some of the same variation in diameter change as packing fraction, matrix density, and particle diameter.

Table 8. ANOVA table of the full model, showing an interaction effect of EFPDs and cumulative fluence for percent change in diameter.

Variable	Sum Sq	Df	F-Value	P-Value
TAVA	1.1415	1	34.7362	9.446E-09
Fluence	2.3252	1	70.7553	1.297E-15
Packing Fraction	0.0505	1	1.5364	0.216
Matrix Density	0.0198	1	0.6031	0.438
Particle Diameter	0.0152	1	0.4626	0.4969
EFPD	0.9083	4	6.9101	2.385E-5
Fluence * EFPD	1.384	3	14.0382	1.257E-08

Figure 11 shows the slope of diameter percent change as a function of cumulative fluence is greater for experiments with shorter irradiation time in EFPDs. If we were to do a multiple comparisons test to compare the slopes among the EFPDs of the four experiments, we would likely see no difference in slope between the experiments with 360.9, 360.23 and 559.18 EFPDs, but the AGR-1 experiment, with 620 EFPDs, would be different from the rest. This could mean that there is an effect of fluence rate, or it could be another confounding factor that differentiates AGR-1 from the rest of the experiments.

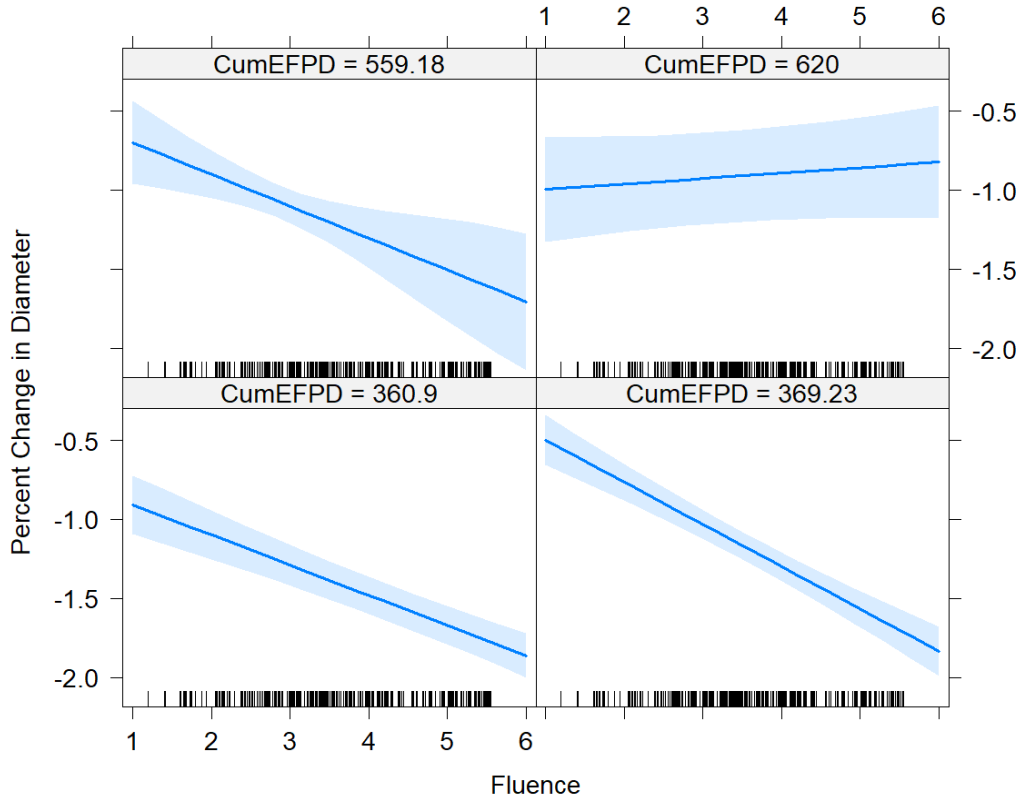


Figure 11. Interaction plot of EFPDs and fluence. Each panel shows the predicted percent change in compact diameter as a function of fluence for the corresponding number of EFPDs for which the compact was irradiated. The light-blue shaded region represents a 95% confidence interval.

We also investigated the effect of fluence rate by creating a new continuous variable by dividing fluence by EFPDs. The results of the model fit with the addition of the continuous effect of fluence rate is given in Table 9.

Table 9. ANOVA table for a full model with continuous effect of fluence rate added for modeling percent change in compact diameter.

Variable	Sum Sq	Df	F-Value	P-Value
TAVA	1.9442	1	54.204	1.44E-12
Fluence	0.0036	1	0.1017	0.7499839
Packing Fraction	0.1526	1	4.2555	0.0399033
Matrix Density	0.0127	1	0.3551	0.5516587
Particle Diameter	0.0415	1	1.1565	0.2829674
Fluence Rate	0.449	1	12.5167	0.0004609

This model also showed a significant effect of fluence rate. The effect plot of the continuous effect of fluence rate (Figure 12) shows the same general trend as the interaction effect given in Figure 11. The higher the fluence rate, the more shrinkage in diameter we see. It is important to note that these models—fit with the variables for fluence rate and matrix grade added to the originally selected model variables—are not necessarily better-fitting models and should not be used for prediction. The intended purpose of fitting these additional models is to make the soundest possible inference on the effects of matrix grade and fluence rate while controlling for other variables that have a demonstrated influence on the change in diameter of a compact.

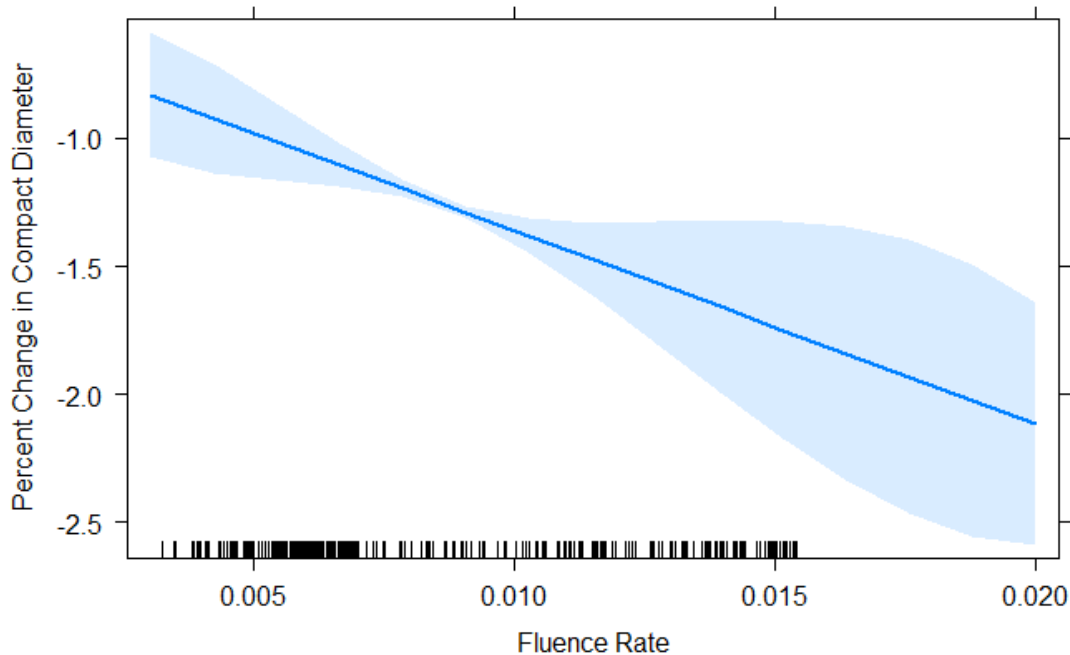


Figure 12. Plot of continuous-fluence-rate effect for model of percent change in compact diameter. X-axis is the fluence divided by 10^{24} divided by the number of EFPDs. The light-blue shaded region represents a 95% confidence interval.

5.1.5. Comparison of model with only fluence vs. full model

During thermal modeling, TAVA is not available, so the thermal calculations use fluence only. We compare a model for percent diameter change as only a function of fluence with the full model presented earlier in this section. The R-squared from the model, using only fluence to predict percent change in compact diameter, is 96%, which is slightly lower than the full model selected above. However, this is still a high R-squared and supports using fluence only as a predictor in the thermal models. Also, to assess the overall fit of the selected model, the predicted values resulting from the model fit were plotted against their corresponding observed percent change in compact diameter as shown in Figure 13.

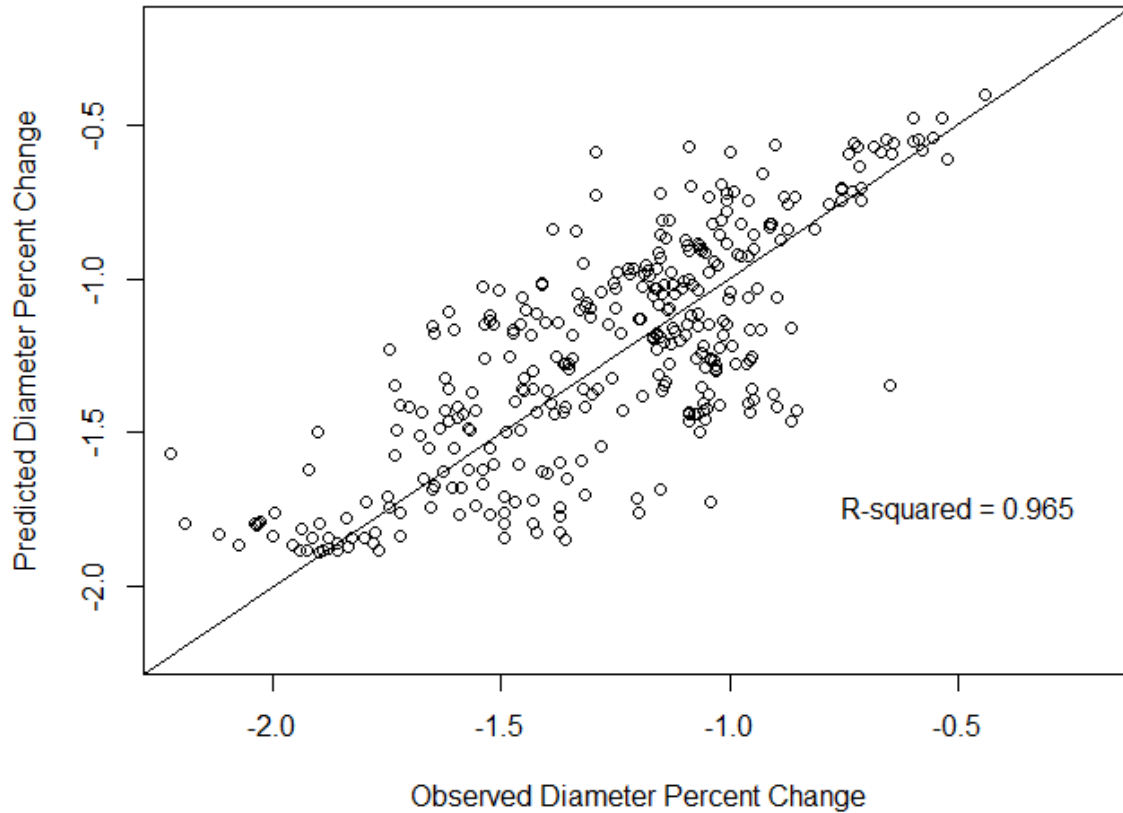


Figure 13. Observed vs. predicted plot for the model predicting compact diameter percent change as function of fluence.

5.2. Change in Compact Length

The next dimensional change that was analyzed is compact length. For comparison, each compact has its percent change in length calculated as from Equation (6).

$$\text{percent change in Length} = \frac{\text{PIE Length} - \text{FAB Length}}{\text{FAB Length}} * 100 \quad (6)$$

Percent change in length was regressed on the same suite of potential variables as described in the analyses of change in diameter; however, diagnostics from the regression fit indicated some heteroscedasticity of residuals which can result in incorrect standard errors for the regression coefficient estimates. Nevertheless, the coefficient estimates themselves remain unbiased. We investigated the impacts of this heteroscedasticity by using a sandwich-type estimator (White 1980) for the covariance matrix of the model to correct the standard errors. Our investigations showed that all coefficient standard errors are slightly overestimated when using the uncorrected linear model approach, and inference remains unchanged. Therefore, we opted to use the same linear-model approach as in the diameter percent change with the caveat that the standard errors for measuring statistical significance of the regression coefficients are slightly inflated, making them more conservative. The analysis of the percent change in length is the same as the diameter analysis.

5.2.1. Fitting data from individual AGR experiments

The models were fitted to the individual AGR data and selected variables for each model using LASSO regression in conjunction with information criteria. The variables selected for each experiment's model are given below in Table 10.

Table 10. Selected variables for linear models for percent change in compact length for each AGR experiment.

Experiment	Variables Selected
AGR-1	TAVA + Fluence
AGR-2	TAVA + Fluence + Packing Fraction + Particle Diameter
AGR-3/4	TAVA + Fluence + Particle Diameter
AGR-5/6/7	TAVA + Fluence + Packing Fraction + Matrix Density

5.2.2. Fitting data from all AGR experiments

We again see that TAVA and fluence are selected as important predictors for each of the AGR experiments. Packing fraction was selected twice, particle diameter and matrix density, each once. We then used LASSO regression to select a global model for the data from all AGR experiments together (Table 11).

Table 11. ANOVA table and parameter estimates from selected model for AGR data for compact length.

Variable	Estimate	Sum Sq	Df	F-Value	P-Value
TAVA	-0.0016266	16.045	1	101.564	2.20E-16
Fluence	0.1903303	7.926	1	50.174	8.46E-12
Packing Fraction	-2.7759527	6.322	1	40.019	8.13E-10
Matrix Density	-0.8081468	3.648	1	23.095	2.34E-06
Particle Diameter	0.0031762	7.726	1	48.904	1.49E-11

The ANOVA table from the selected global model shows the same variables were selected for the length percent change model as were for the diameter model. The sums of squares and p-values again indicate that TAVA and fluence are the most-important predictors, followed by particle diameter, packing fraction, and matrix density.

To visualize the effects of the variables selected in the ANOVA in Table 10, we give an effects plot in Figure 14. Higher TAVA led to greater shrinkage in compact length; however, fluence had a positive effect on compact length whereas it had a negative effect on diameter change. The effects plot indicates that the length of a compact shrinks less (or may even increase) as fluence increases. Also, we see that the packing fraction effect on change in length is opposite of the effect on diameter. The effects of matrix density and particle diameter maintain the same direction as their effects on diameter change.

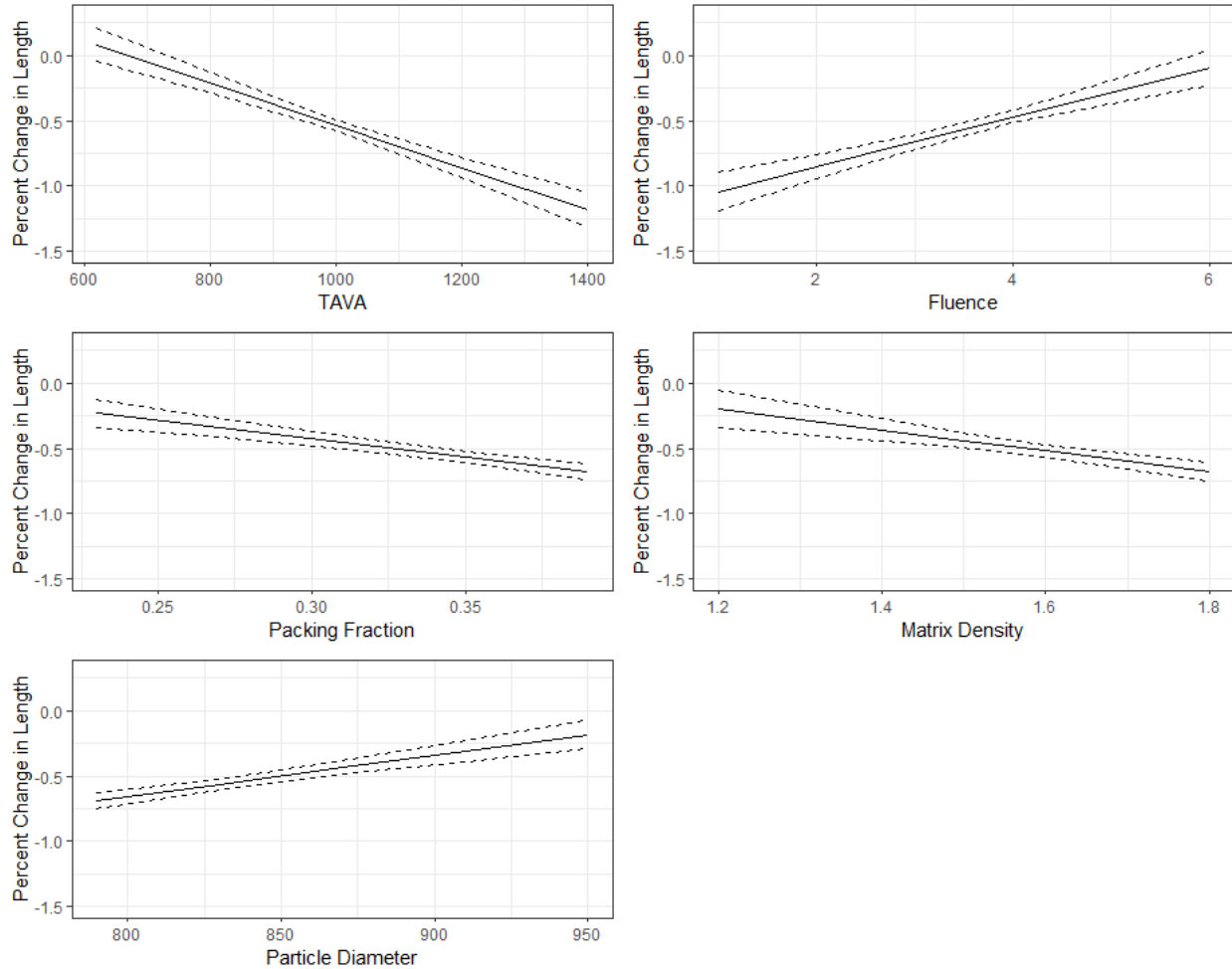


Figure 14. Effects plots for variables selected for the model of percent change in compact length.

The model fit had a lower R-squared of 73% as compared to the 98% of the diameter-change analysis, indicating there may be other factors influencing the change in the length of compacts that we have not accounted for in our model. The model residuals had a mean close to zero of $1.6\text{E-}3$ and a plot of observed-versus-predicted values for percent change in length indicates no systematic bias in prediction (Figure 15). The data points are more scattered about the 1:1 line—hence the lower R-squared value—specifically, the AGR-5/6/7 data have more points farther from the 1:1 line than the other experiments. This likely indicates we have not accounted for some factor influencing the variation of percent change in length in the AGR-5/6/7 experiment. One possibility could be that the graphite used for the matrix material in AGR-5/6/7 was different from the other experiments, and the response in the length direction of this graphite to irradiation is more variable than the graphite used in the other experiments.

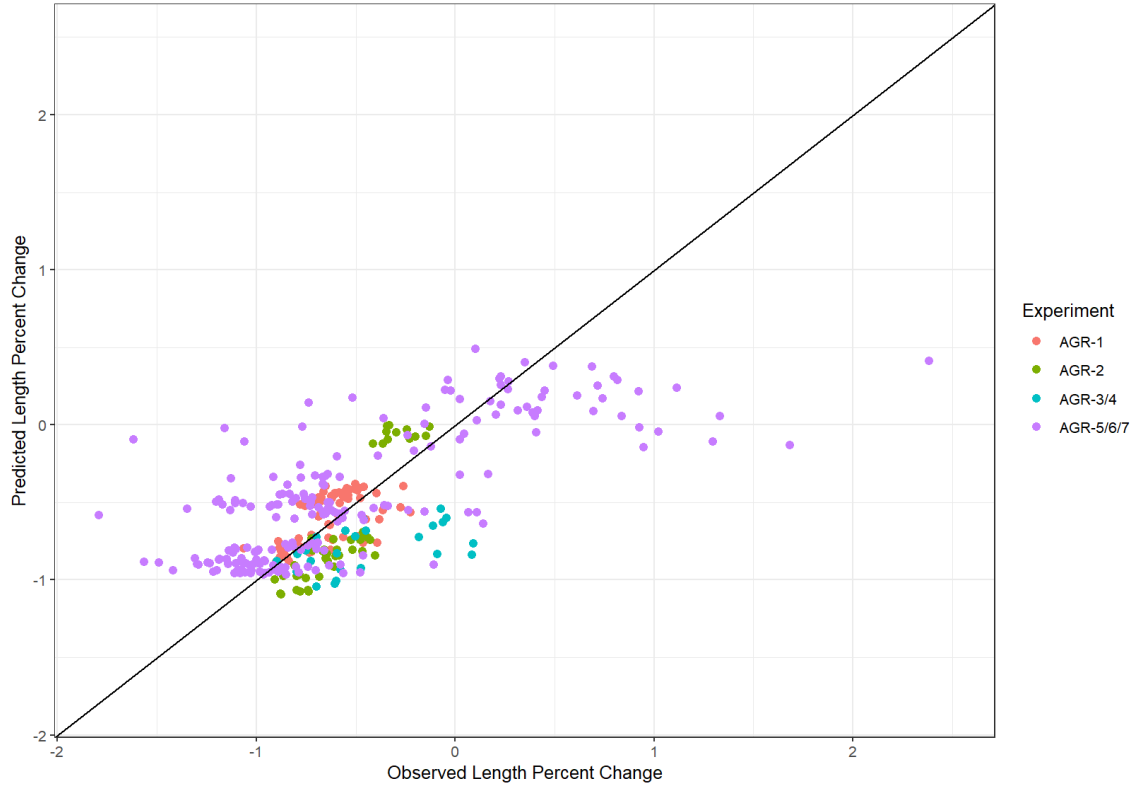


Figure 15. Plot of observed versus predicted values for percent change in compact length for AGR experiments. The black line represents the 1:1 line where all points should lie in the unrealistic case of a perfect fit.

5.2.3. Investigating influence of the compact-matrix graphite grade

The results from the model fitted with the inclusion of a factor for matrix grade indicate there is significant variation in percent change in length explained by matrix grade ($p\text{-value} = 1.29\text{E-}15$). All the variables in Table 12 indicate statistical significance, even with the addition of a matrix-grade effect. This supports our observation from the observed versus predicted plot that the AGR-5/6/7 compacts may be different from the rest because the matrix grade, again, is essentially comparing AGR-5/6/7 to all other experiments. The effect of matrix grade on the compact-length shrinkage is plotted in Figure 16.

Table 12. ANOVA table for percent change in length with a factor for matrix grade incorporated.

Variable	Sum Sq	Df	F-Value	P-Value
TAVA	20.266	1	156.9658	2.20E-16
Fluence	4.413	1	34.1815	1.21E-08
Packing Fraction	4.238	1	32.8223	2.28E-08
Matrix Density	2.916	1	22.5827	3.01E-06
Particle Diameter	1.176	1	9.1051	0.002747
Matrix Grade	9.841	2	38.1094	1.29E-15

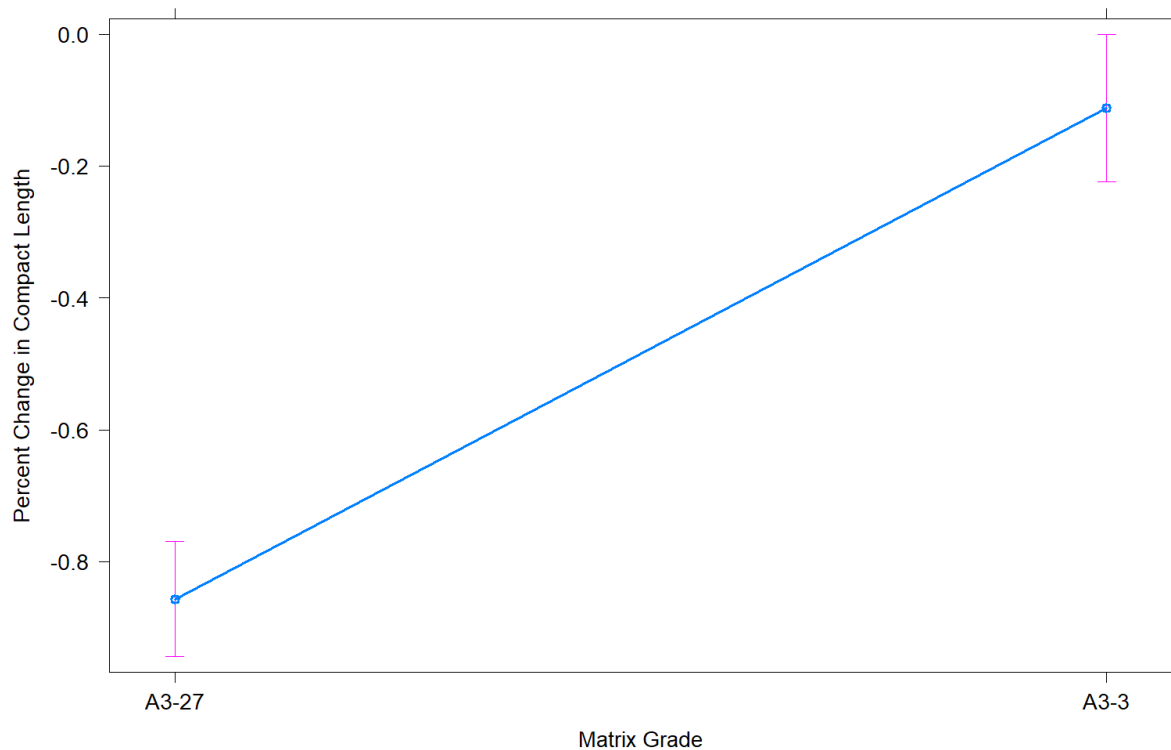


Figure 16. Effect plot of matrix grade on percent change in compact length.

5.2.4. Investigating influence of the fluence rate

The effect of fluence rate is investigated by removing the matrix-grade variable and including a main effect for EFPDs and an interaction of fluence with EFPDs. The ANOVA model summary is presented in Table 13.

Table 13. ANOVA of model for percent change in length with incorporation of EFPDs and an interaction effect to test for a fluence rate effect.

Variable	Sum Sq	Df	F-Value	P-Value
TAVA	18.015	1	148.0459	2.20E-16
Fluence	4.159	1	34.1808	1.22E-08
Packing Fraction	5.415	1	44.5005	1.10E-10
Matrix Density	0.088	1	0.7196	0.3968896
Particle Diameter	2.174	1	17.8662	3.08E-05
EFPD	10.701	4	21.9844	4.48E-16
Fluence*EFPD	2.2	3	6.0252	0.0005273

The interaction effect of fluence and EFPDs in Table 12 is statistically significant, so we visualize this with an interaction effect plot to better understand the effect (Figure 17).

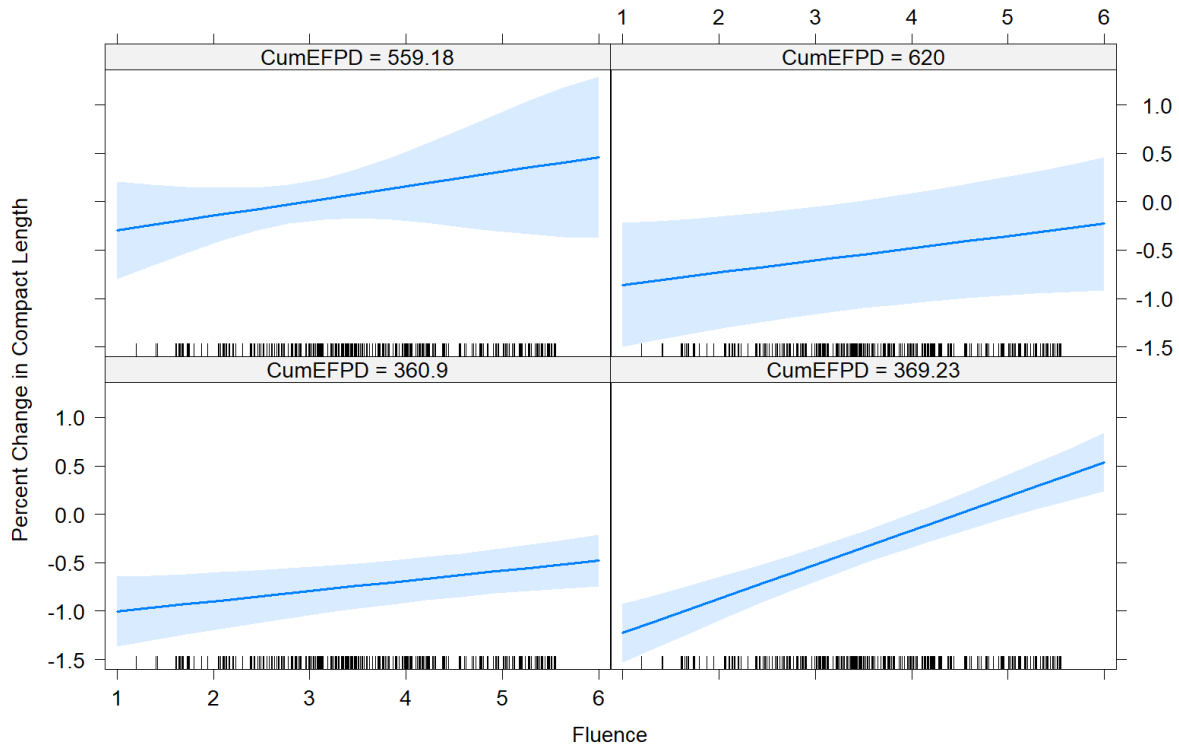


Figure 17. Interaction effect plot for EFPDs with fluence on percent change in compact length.

The effect plot in Figure 17 indicates all the compacts in the different experiments shrunk in length less at higher fluences, but the AGR-3/4 experiment (with 369.23 EFPDs) exhibited a slightly stronger effect of fluence on percent change in length. To assess this differently we included a continuous variable for fluence rate as well (Table 14).

Table 14. ANOVA for percent change in length with added effect of fluence rate.

Variable	Sum Sq	Df	F-Value	P-Value
TAVA	16.041	1	101.2753	2.20E-16
Fluence	0.575	1	3.6275	0.0577
Packing Fraction	6.31	1	39.8368	8.87E-10
Matrix Density	0.186	1	1.1764	0.27888
Particle Diameter	0.864	1	5.4517	0.02015
Fluence Rate	0.02	1	0.1272	0.72157

The effect of fluence rate is not significant for predicting percent change in compact length. An effect plot (Figure 18) indicates a slightly negative relationship of fluence rate with percent change in compact length, but it is not statistically significant indicated by the wide 95% confidence limits and relatively flat line (i.e., slope not different from zero).

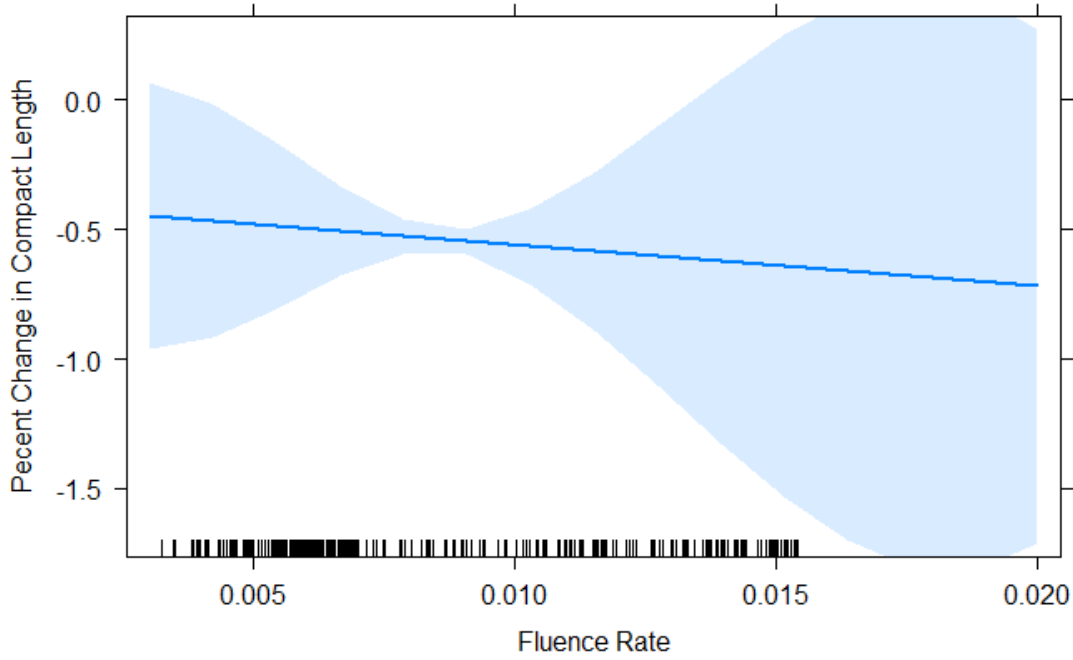


Figure 18. Effect plot for fluence rate on diameter percent change. Light-blue shaded area represents 95% confidence limits.

The analysis of the percent change in length was similar in the variables that were selected as important predictors of change in diameter; however, some of the relationships, such as fluence with length change, were opposite of the effects with diameter change. This was likely partially caused by a less-well-fit model for the global model selected and the reduced R-squared value. The AGR-5/6/7 data exhibited more variation in the percent change in length than did the other experiments. AGR-5/6/7 data had 45 compacts that increased in length while there were only two compacts in AGR-3/4 that increased in length after irradiation. None of the AGR-1 or AGR-2 compacts increased in length.

5.3. Change in Compact Volume

Analysis for percent change in volume was carried out using the same process as for length and diameter. We used LASSO regression and information criteria to select the most important variables by experiment then selected a set of variables for the experiments combined. Percent change in volume was expressed as:

$$\text{percent change in volume} = \frac{\text{PIE volume} - \text{FAB volume}}{\text{FAB volume}} * 100 \quad (8)$$

5.3.1. Fitting data from individual AGR experiments

The models were fitted to the individual AGR data and selected variables for each model using LASSO regression in conjunction with information criteria. The variables selected for each experiment's model are given below in Table 15. The variables selected for each experiment's model were similar for volume as for diameter and length. TAVA and packing fraction were selected for each experiment, with fluence selected in three, and matrix density and particle diameter in two.

Table 15. Variables selected for models of volume percent change fit to each experiment separately.

Experiment	Variables Selected
AGR-1	TAVA + Fluence + Packing Fraction + Matrix Density + Particle Diameter
AGR-2	TAVA + Fluence + Packing Fraction + Particle Diameter
AGR-3/4	TAVA + Packing Fraction
AGR-5/6/7	TAVA + Fluence + Packing Fraction + Matrix Density

5.3.2. Fitting data from all AGR experiments

The models were fitted to all AGR data combined, and variables were selected for the model using LASSO regression in conjunction with information criteria. The results of the LASSO regression-variable selection for volume percent change are given in Table 16.

Table 16. ANOVA table and coefficient estimates for selected model fit to all AGR experiments for percent volume change.

Variable	Estimate	Sum Sq	Df	F-Value	P-Value
TAVA	-0.00269	43.758	1	136.6113	2.20E-16
Fluence	-0.17406	6.629	1	20.6949	7.56E-06
Packing Fraction	-1.90387	2.974	1	9.2841	0.002497
Matrix Density	-2.25371	28.374	1	88.5834	2.20E-16
Particle Diameter	0.005491	23.091	1	72.0892	6.97E-16

The variables selected to explain the greatest variation in percent change in compact volume were again the same as for diameter and length. TAVA was the most significant variable, followed by matrix density and particle diameter. Fluence and packing fraction were the least significant variables according to the ANOVA table; however, an effects plot is useful to assess the magnitude of the estimated effects (Figure 19).

We see again similar relationships between our five predictor variables and the change in compact volume. This is expected because volume is correlated with length and diameter as it is a function of both metrics. Fluence, temperature, packing fraction, and matrix density are inversely related to volume change while particle diameter is positively related. In other words, the compacts shrink more as fluence, temperature, packing fraction, and matrix density increase while compacts shrink less as particle diameter increases. To further investigate the effect of matrix grade, we again added an effect for matrix grade, essentially comparing AGR-5/6/7 to the other AGR experiments.

The model selected for percent volume change was the same as for the diameter and length percent change and resulted in a fit with an R-squared of 97%. The observed versus predicted plot shows no systematic bias in estimation, suggesting the model fits well and should provide reliable inferences. The model residuals had a mean close to zero of $1.7\text{E-}3$, and a plot of observed-versus-predicted values for percent change in volume indicates no systematic bias in prediction (Figure 20).

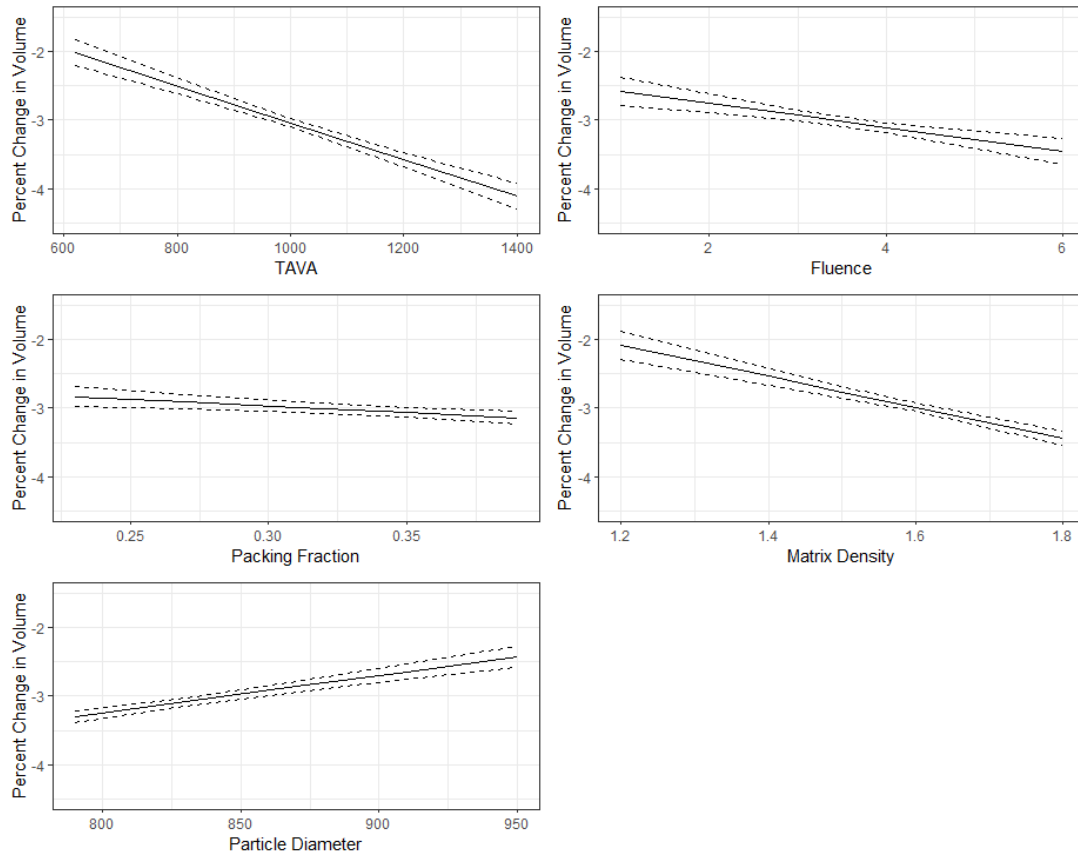


Figure 19. Effects plot for selected model of percent change in compact volume.

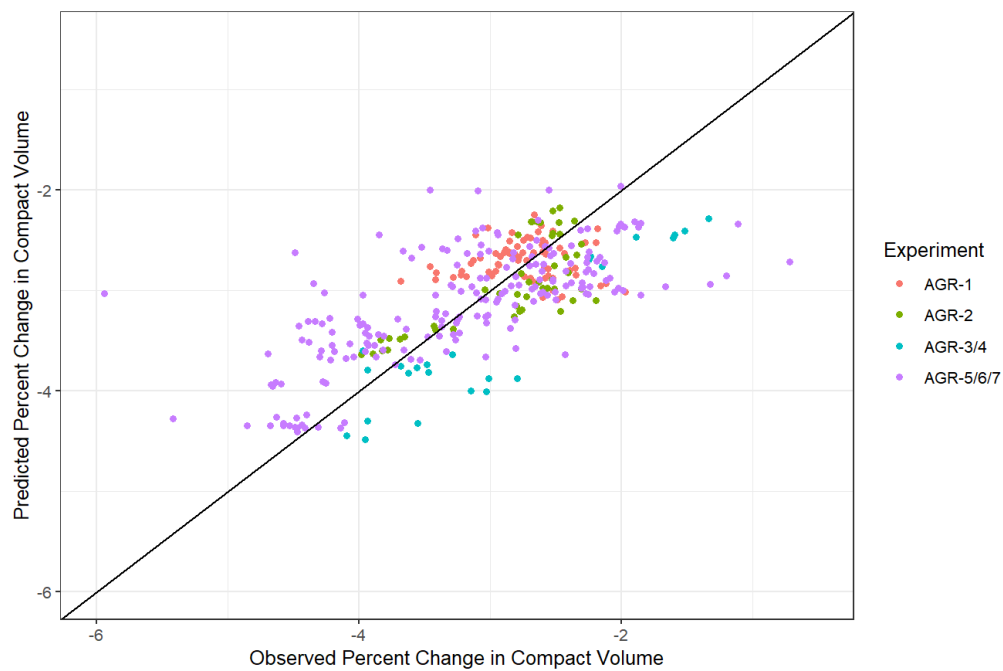


Figure 20. Observed versus predicted percent change in compact volume for model fit.

5.3.3. Investigate influence of the compact matrix graphite grade

To assess the effect of the difference in matrix grade used for AGR-5/6/7 versus the other AGR experiments, we added a categorical predictor for matrix grade. The results of the fit with the new predictor added are given in Table 17.

Table 17. ANOVA table of model fit with categorical predictor for matrix grade.

Variable	Sum Sq	Df	F-Value	P-Value
Mean TAVA	50.234	1	180.7221	2.20E-16
Fluence	2.922	1	10.5128	0.001307
Packing Fraction	2.085	1	7.5001	0.006504
Matrix Density	0.313	1	1.1259	0.28942
Particle Diameter	0.387	1	1.3931	0.238735
Matrix Grade	14.614	2	26.2883	2.55E-11

The ANOVA given in Table 17 indicates a significant effect of matrix grade on volume change. We also notice that matrix density and particle diameter are no longer significant predictors, indicating some possible confounding. An effects plot of matrix grade helps us interpret the effect. The effects plot of matrix grade (Figure 21) indicates that the AGR-5/6/7 compacts with the A3-27 matrix material shrank on average 3.44% while compacts of the A3-3 material only shrank 2.51% in volume.

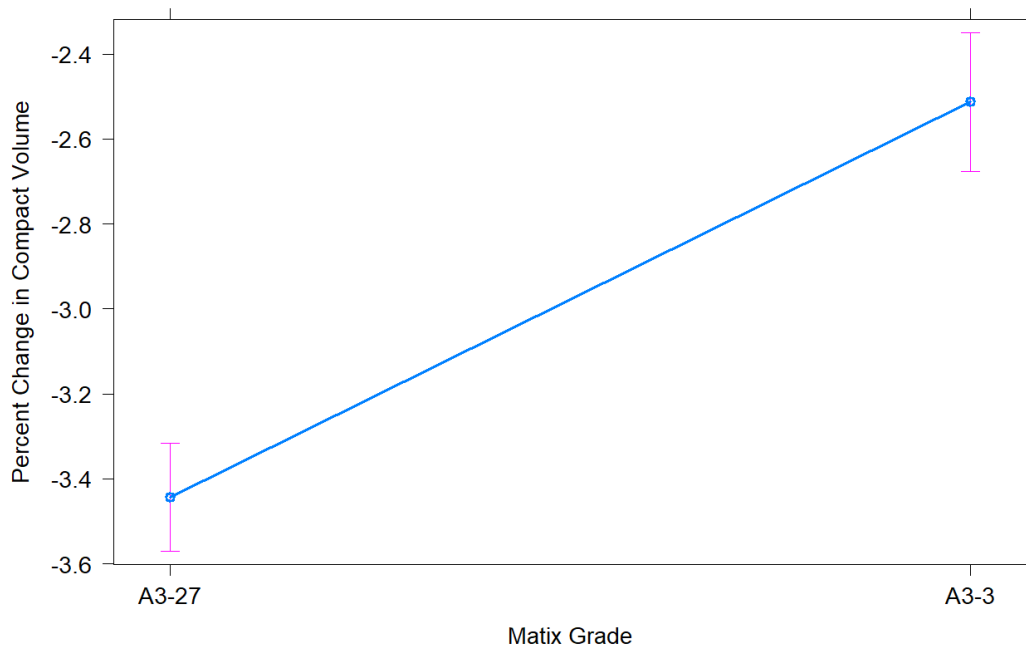


Figure 21. Effect plot of matrix grade for model fit to volume percent change.

5.3.4. Investigate influence of the fluence rate

To investigate the effect of fluence rate, we included a categorical predictor for EFPDs as well as an interaction EFPDs with cumulative fluence. The results of this model fit to predict percent volume change are given in Table 18.

Table 18. ANOVA table showing the main effect of EFPD and an interaction effect of EFPD with fluence.

Variable	Sum Sq	Df	F-Value	P-Value
TAVA	38.51	1	142.9984	2.20E-16
Fluence	2.79	1	10.3605	0.001417
Packing Fraction	3.342	1	12.4084	0.000489
Matrix Density	0.319	1	1.1861	0.276928
Particle Diameter	1.419	1	5.2699	0.022333
EFPD	15.171	4	14.0837	1.31E-10
Fluence*EFPD	3.648	3	4.5148	0.004049

The interaction effect of fluence with EFPD was statistically significant, indicating some difference in volume change as a function of EFPD and fluence. This effect, as noted in previous analyses, is confounded with the experiment so that other experiment-specific factors not accounted for here could also be the cause of this significant result. To better understand the interaction effect, the two lower plots in the panel in Figure 22 indicate that the two experiments with shorter irradiation time (AGR-3/4 and AGR-5/6/7) had slightly more volumetric shrinkage as fluence increased. The upper two plots indicate that the experiments that were irradiated for longer (AGR-1 and AGR-2) showed less volumetric shrinkage as a function of fluence.

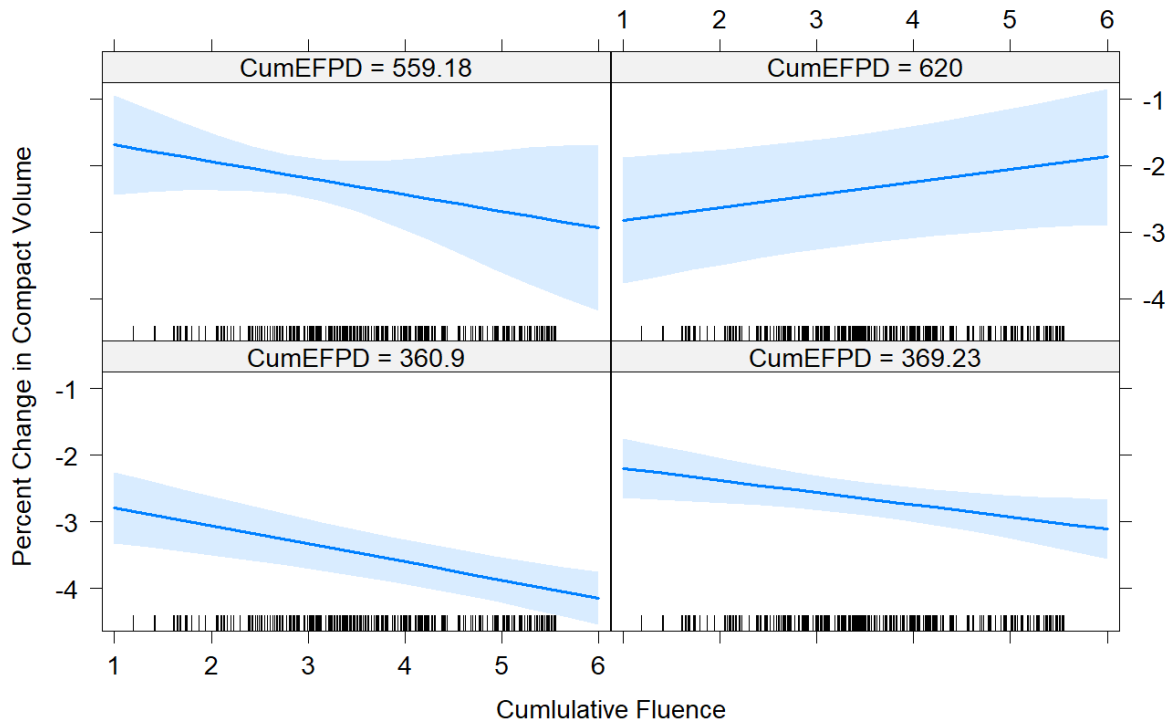


Figure 22. Effect plot for the interaction of EFPD with fluence to predict percent change in volume.

To assess the effect of fluence rate in another way, the continuous effect of fluence rate as calculated by dividing fluence by EFPD was investigated (Table 19). We see a significant effect of fluence rate when included with the other variables we found to be important predictors of volume change. A plot of this effect helps us interpret the effect of fluence rate as a continuous predictor (Figure 23).

Table 19. ANOVA table resulting from fit of model including continuous effect of fluence rate on percent volume change.

Variable	Sum Sq	Df	F-Value	P-Value
TAVA	43.703	1	138.8028	2.20E-16
Fluence	0.733	1	2.3272	0.128089
Packing Fraction	2.898	1	9.2031	2.61E-03
Matrix Density	0.036	1	0.1138	0.736095
Particle Diameter	0.236	1	0.7483	0.387645
Fluence Rate	2.127	1	6.7543	0.009771

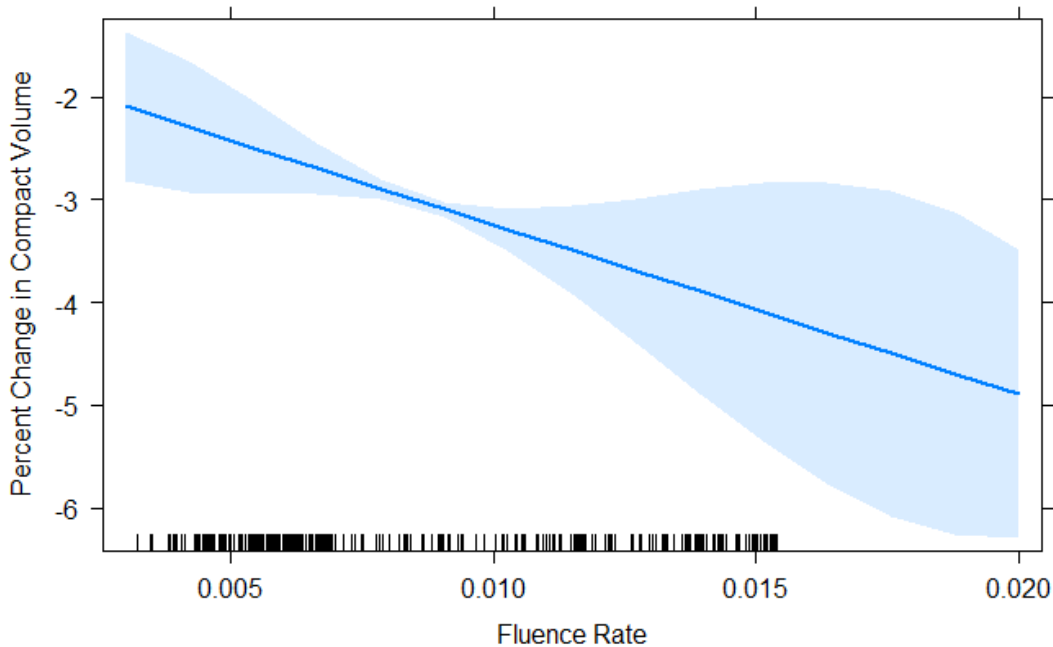


Figure 23. Effect plot of fluence rate as continuous predictor of percent volume change. Shaded, light blue area indicates 95% confidence limits.

The effect plot of fluence rate indicates the same relationship we saw for diameter and length percent change; compacts that were irradiated at higher fluence rates shrank more. It is important to caution here that the effect of matrix grade from the AGR-5/6/7 experiment may be partially driving this effect; we know the AGR-5/6/7 compacts shrank slightly more than the rest on average, and AGR-5/6/7 was irradiated for a shorter number of EFPD. Thus, this could partially be an artifact of the matrix material difference between experiments.

6. DISCUSSION

It is well-known that graphite material shrinks at lower fluence and then starts to expand at higher fluence (so called turnaround fluence) (Burchell and Snead 2007). The goal of this analysis was to determine manufacturing variables and irradiation condition variables that influence irradiation-induced dimensional change in AGR TRISO fuel compacts and to infer their effects.

6.1. Different Dimension Change Behavior for Individual AGR Experiments

As described throughout the document, confounding factors among the different capsules and experiments (i.e., AGR-1, AGR-2, AGR-3/4, and AGR-5/6/7) make it difficult to make broad inferences on these variables across all the experiments. Therefore, our interpretations must be made with some caution. Some of the confounding factors that we are aware of for manufacturing variables are particle diameter which was intentionally smaller for AGR-1 and AGR-3/4 than AGR-2 and AGR-5/6/7. Also, matrix density was particularly high for AGR-5/6/7 compared to AGR-1. Perhaps the most confounded factor was the grade of matrix material used in AGR-5/6/7 compared to the other experiments. There are also concerns with confounding's making causal inference challenging due to irradiation conditions, such as fluence and temperature, differing among experiments in addition to the manufacturing differences between experiments. Even while taking these confounding factors into consideration, some inferences can be made on the overall impacts of the variables considered here.

The three panel plots (Figure 24 through Figure 26) show the change in diameter, length, and volume as a function of fluence and color-coded by temperature for each experiment. Increases in fluence were associated with more shrinkage for diameter and volume (more-negative changes, as shown in Figure 23 and Figure 25) for all compacts; however, the length-change plots (Figure 24) indicated that increased fluence resulted in less shrinkage or even growth in length for numerous compacts. Therefore, the turnaround fluence was not reached for the diameter and volume because all compacts had smaller PIE diameters and volumes than as-fabricated, but there were 45 AGR-5/6/7 and two AGR-3/4 compacts which increased in PIE length.

Many AGR-5/6/7 compacts (see bottom right plot of Figure 24) at lower temperatures and higher fluence increased in length. This could be indicative of an interaction effect of TAVA temperature and fluence because the hotter compacts at higher fluences exhibited more diameter reduction than cooler compacts at similar fluences. This begins to look like turnaround in the compact diameter occurs at lower fluences for cooler fuel than for hotter fuel; however, this hypothesis is difficult to test using these data because, to really understand the process, we would want replicates of compacts measured at different temperatures across the whole range of fluences. Furthermore, it would contradict findings in literature (Marsden et al. 2016), which showed that the higher the irradiation temperature, the lower the fluence of the turnaround. Also, a comparison of the AGR-5/6/7 plot and the AGR-3/4 plot shows that the hottest compacts in AGR-3/4 appear to possibly have achieved turnaround and increased in length. Based on the information (if available) on the turnaround point as a function of dose and temperature for the grade of irradiated graphite, a more-appropriate model, including a quadratic effect of fluence, can be studied or possibly break the regression into pre- and post-shrinkage turnaround.

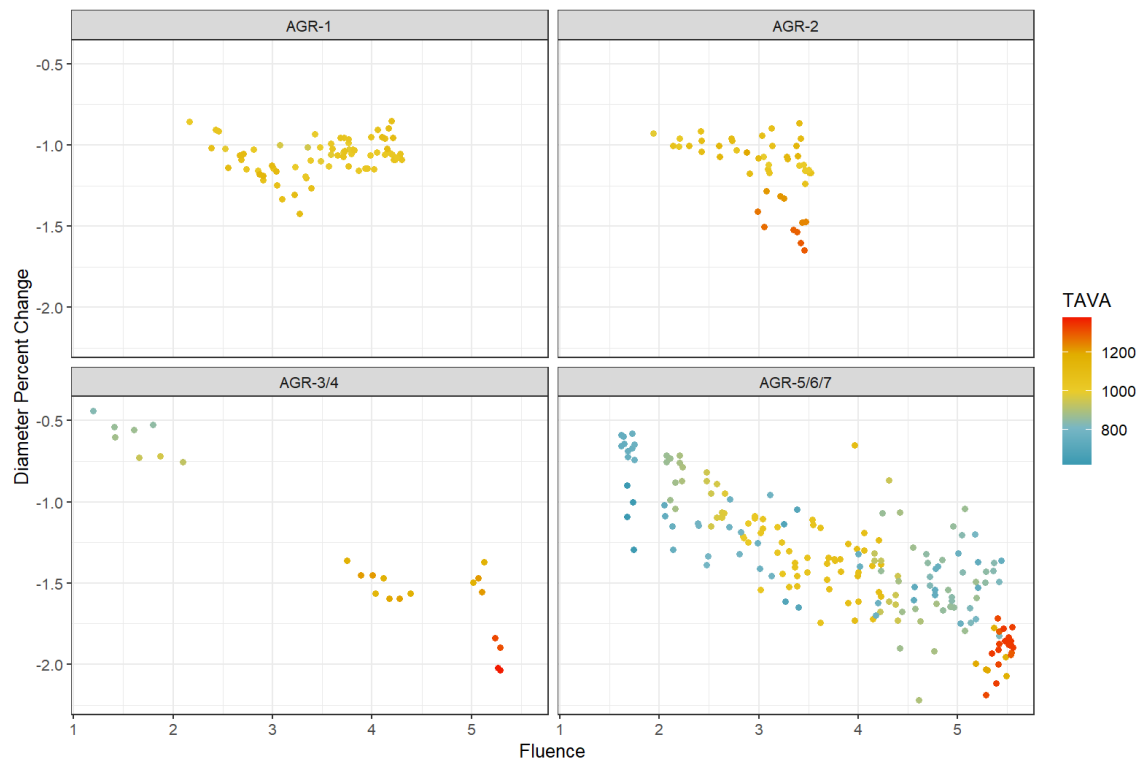


Figure 24. Percent change in diameter as a function of fluence and TAVA temperature by experiment.

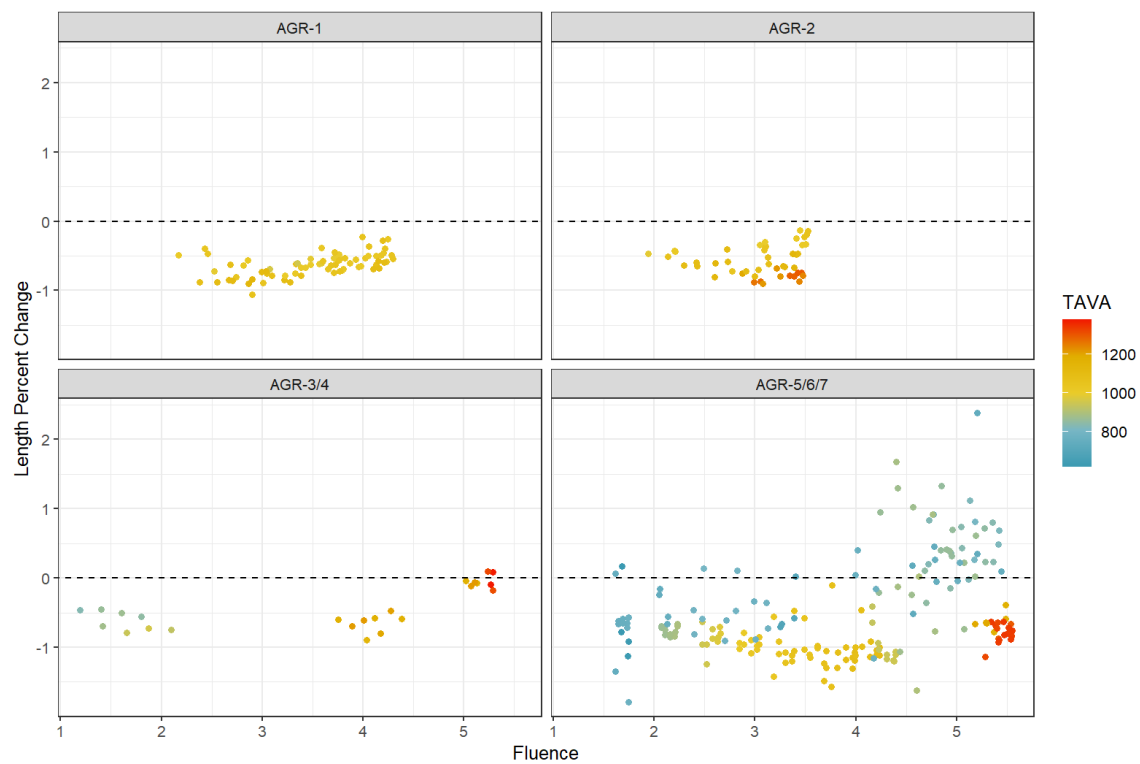


Figure 25. Percent change in length as a function of fluence and TAVA temperature by experiment.

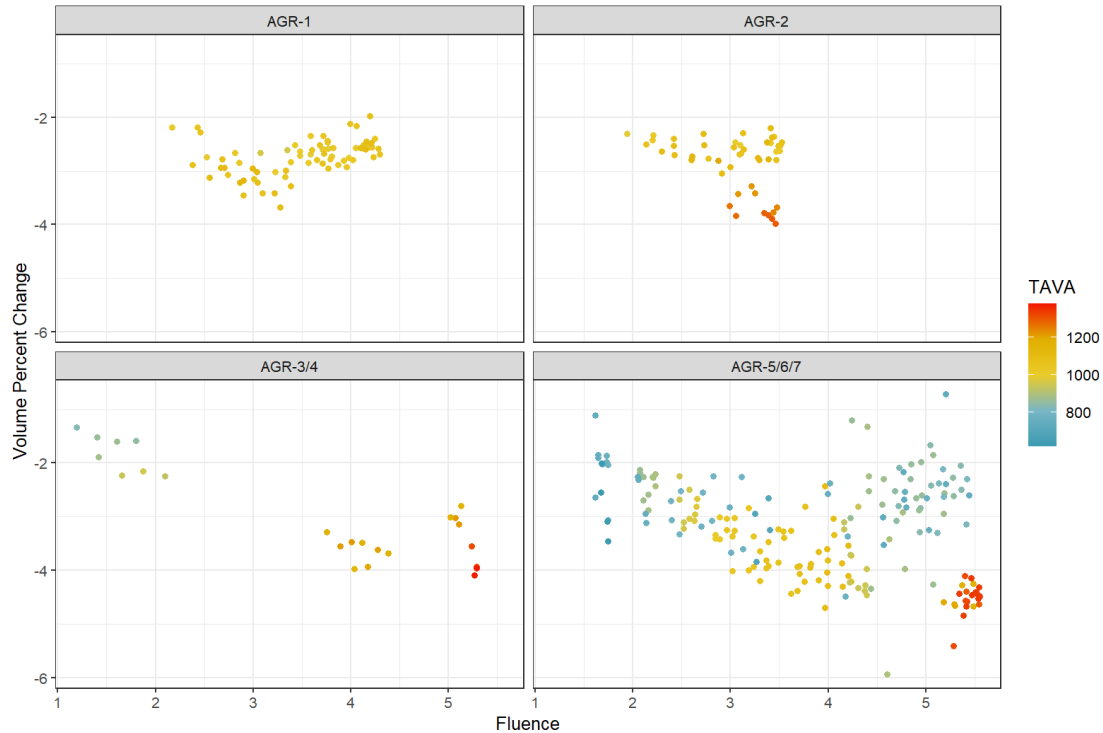


Figure 26. Percent change in volume as a function of fluence and TAVA temperature by experiment.

The addition of the categorical predictor for matrix grade was also significant for each dimensional model. Even with the likelihood that some AGR-3/4 and AGR-5/6/7 compacts began to pass the turnaround point of shrinkage in length, the AGR-5/6/7 compacts, with the A3-27 matrix, presented lengths that shrank more on average than comparable compacts of the other AGRs with A3-3 matrix.

6.2. Dimensional Change for all AGR Experiments

Initial variable selection to reduce collinearity of the independent variables suggested that matrix density was a better predictor than overall compact density. Also, TAVA temperature was selected over minimum TA and maximum TA temperature as a slightly better predictor for dimensional change. The coefficient estimates for each variable from the three-dimensional change models are shown in Table 20. The same variables were selected as important for each dimensional change; however, this does not mean these are the only variables that are important to compact dimensional change or that there are no interactions present among these main effects. Overall, the models indicated satisfactory fits to each data set, with R-squared values of 98%, 74% and 97% for diameter, length, and volume percent change models respectively, and well-behaved residuals.

Table 20. Regression coefficients for percent change in diameter, length, and volume models.

Variable	Regression Model		
	% Change in Diameter	% Change in Length	% Change in Volume
Mean TAVA Temperature per Compact (°C)	-0.000567	-0.0016266	-0.00269
Fast Fluence/1025 ($E > 0.18$ MeV) (n/m^2)	-0.1822	0.1903303	-0.17406
Compact Packing Fraction	0.4202	-2.7759527	-1.90387
FAB Matrix Density (g/cm^3) TAVA	-0.7508	-0.8081468	-2.25371
TRISO Fuel Particle Diameter (μm)	0.001245	0.0031762	0.005491

As expected, mean TAVA temperature and fast-neutron fluence were the two main predictors that had the largest and most-significant slope coefficients for change in each dimension. This was demonstrated in the effects plots in the previous sections. Matrix density was probably the third most important predictor of all dimensional change, followed by particle diameter and packing fraction. Though packing fraction and particle diameter were found to be statistically significant, their effect sizes were smaller than other factors. We also note that the direction of the packing-fraction effect is positive for change in diameter, but negative for length and volume. This is not terribly surprising because it is a small effect to begin with; thus, a small amount of confounding or other changes could cause this coefficient to switch directions.

Figure 27 through Figure 29 show the percent change in compact dimensions for all compacts together to better visualize the behavior of all the data combined as a function of fluence and TAVA. Irradiation-induced compact diameter (Figure 27) and volume (Figure 29) changes, increasing with increase in of fluence, is consistent across the four AGR experiments. However, diameter change rates for AGR-1 compacts (circle symbols at $\sim 1000^{\circ}\text{C}$ VATA) are in lesser tendency. In contrast, compact length changes (Figure 28) do not exhibit similar trend, especially PIE lengths of quite a few of compacts were even longer than their as-fabricated values as stated in the previous subsection.

At the same time, a similar trend of compact dimension changes as function of TAVA for the three dimensions (diameter, length, and volumes) is also observable. Specifically, increase in diameter and volume shrinkages is associated with an increase in TAVA temperature but that trend is not apparent for the length shrinkage.

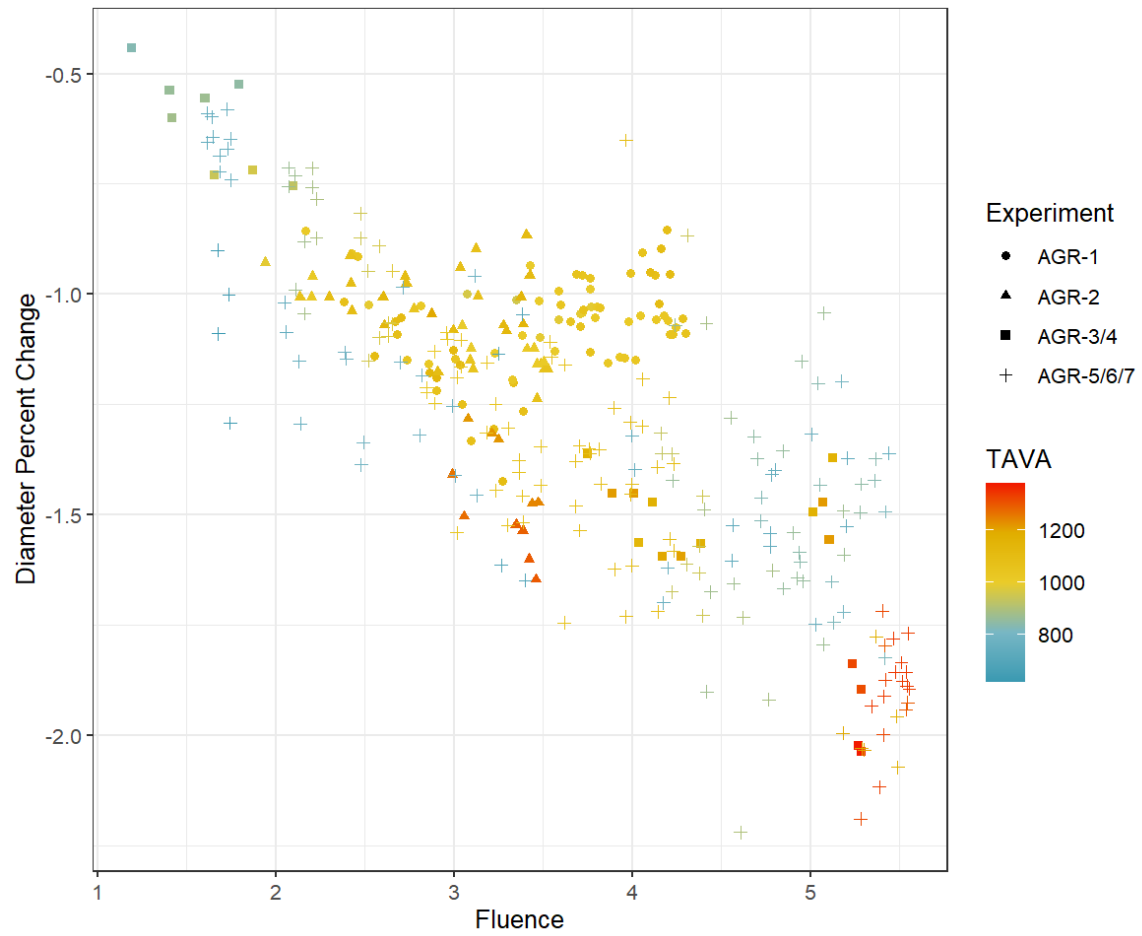


Figure 27. Percent change in diameter of all compacts as a function of fluence. The color of points indicates TAVA, and the shapes indicate the experiment to which the compact belongs.

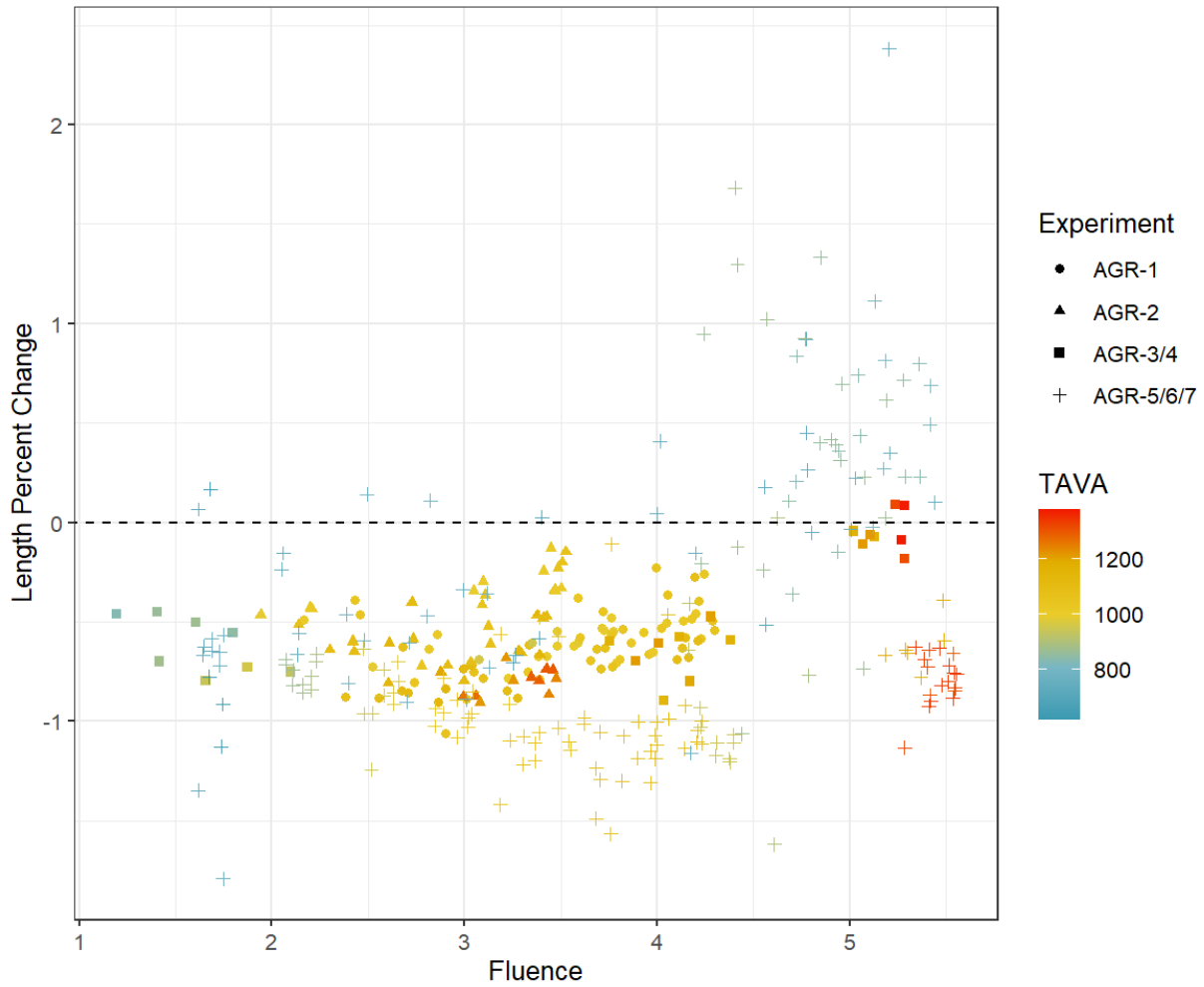


Figure 28. Percent change in length of all compacts as a function of fluence. The color of points indicates TAVA, and the shapes indicate the experiment to which the compact belongs.

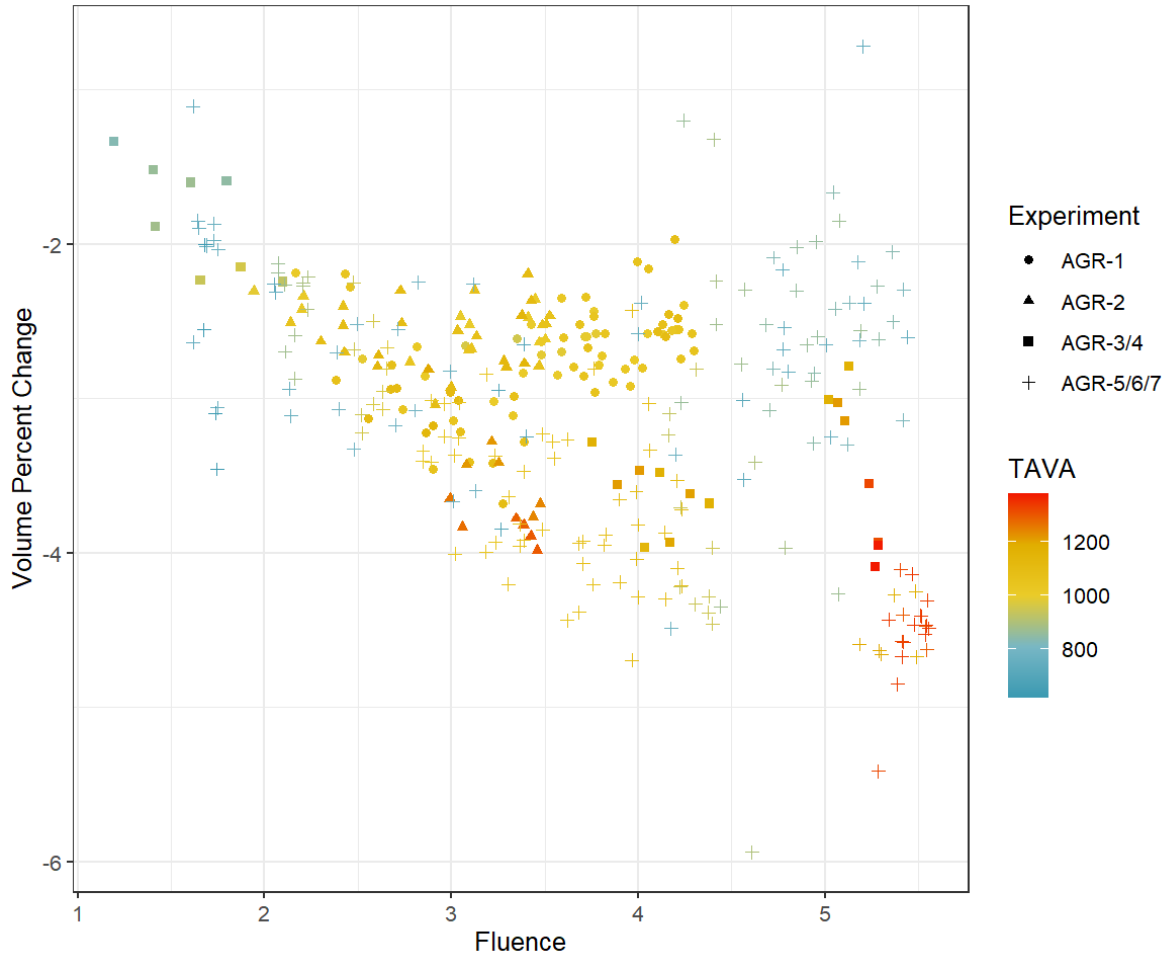


Figure 29. Percent change in volume of all compacts as a function of fluence. The color of points indicates TAVA, and the shapes indicate the experiment to which the compact belongs.

In all the models for three dimensions (diameter, length, and volumes), an increase in mean TAVA temperature was associated with greater shrinkage. Matrix density was also negatively correlated with each dimensional change, indicating an increase in matrix density was associated with greater shrinkage in each compact dimension. This should be interpreted carefully because we know that AGR-5/6/7, which had the highest matrix density of the experiments, may be driving this effect due to the different matrix material used. TRISO-particle diameter was positively associated with percent change for each of the three dimensions, indicating larger particles result in less shrinkage. Again, we must be cautious here because AGR-5/6/7 had the largest particles, which were not measured individually; rather, the nominal value of 847.35 was assigned to all particles (Table 4). Therefore, particle size is potentially confounded with experimental differences of AGR-5/6/7. Packing fraction was considered as a continuous variable because it can take on any real number between zero and one; however, the various compacts in the different experiments were designed to have fuel consisting of a particular packing fraction, matrix density, compact density, and particle diameter within some specified range. Therefore, these variables may be better suited for analysis if binned or grouped and used as categorical variables.

Also, the fluence rate seemed to influence the percent change of all three dimensions. On average, the compacts that reached the same fluence at faster rates (i.e., had shorter irradiation time) shrank slightly more than compacts that were irradiated longer. This could be important if the irradiation testing in ATR is meant to demonstrate how fuels and reactor components would respond in a commercial reactor, and fluence rate does indeed affect dimensional change, it may be necessary to account for this when predicting what to expect in dimensional change in fuels and components in a commercial reactor. Nevertheless, this effect must be interpreted cautiously because the matrix grade could be the driving factor for this difference. This is because AGR-5/6/7 had a high fluence rate and more shrinkage than the other experiments at the same temperatures.

7. CONCLUSION

Overall, we have demonstrated with linear main-effects models that TAVA temperature, fluence, TRISO fuel-particle diameter, matrix density, and packing fraction are factors that are important for predicting how fuel compacts change in dimensions in a reactor. The variables selected as important in this analysis were also selected as important in the previous version of this analysis, which used the same data set, but also including AGC-2 and not including the AGR-5/6/7 data. In contrast to the previous analysis, we also found that there may be a difference in dimensional change due to the type of matrix material used and the rate at which fast-neutron fluence was accrued. In general, all data from all experiments, including AGC-2 (although not formally analyzed here) behaved similarly in percent change in compact diameter: all compacts consistently shrunk; however, there were some differences in the change in compact length and volume among experiments. AGR-5/6/7 compacts showed significant variation in the percent change in length of compacts. A linear model for predicting percent change in diameter as solely a function of fluence was compared to the global model selected here. Results indicated that the global model is slightly better (R-squared of 96% for fluence only vs. 98% for global model), however a model using only fluence, as is done for the thermal calculations, does perform well.

In all dimensional directions (i.e., length and diameter), TAVA and matrix density were negatively associated with dimensional change while particle diameter was positively associated. Packing fraction showed perhaps the weakest, but statistically significant, relationship with dimensional change and was positively associated with changes in diameter while negatively associated with changes in length and volume. We attribute this inconsistent relationship between packing fraction and dimensional change to the relatively small effect of packing fraction relative to other factors. Fluence was negatively associated with diameter and volume change while positively associated with changes in length. This may be an artifact of compacts' in AGR-3/4 and especially AGR-5/6/7 experiencing dimensional turnaround as a function of irradiation dose. Future investigations of these data should assess whether the turnaround point of that matrix material was likely reached and incorporate the anticipated turnaround point into the model. We assumed a linear relationship of all variables with dimensional change; however, if turnaround was indeed reached, a model for pre- and post-turnaround may be more appropriate. The A3-3 matrix material used in the AGR-1, 2, and 3/4 showed less shrinkage in each dimension relative to the A3-27 material used in the AGR-5/6/7 compacts. A variable derived for fluence rate by dividing fluence by EFPDs was also found to be negatively associated with changes in all three dimensions.

These results are useful; however, the many confounding factors among experiments suggest individual models for each experiment may be beneficial. The AGR-5/6/7 data stand out with lower mean TAVA temperatures for many compacts and a different matrix grade, which suggests a model for AGR-5/6/7 data might be useful. The analyses presented here support the findings of the previous version of this analysis, and the variables selected as important predictors and their relationships with dimensional change will be useful for future planning of irradiation events.

8. REFERENCES

- Burchell, T. D. and Snead, L. L., 2007. "The effect of neutron irradiation damage on the properties of grade NBG-10 graphite." *Journal of Nuclear Materials* 371(1–3): 18–27.
<https://doi.org/10.1016/j.jnucmat.2007.05.021>.
- Collin, B. P., 2015a. "AGR-1 Irradiation Test Final As-Run Report." INL/EXT-10-18097, Idaho National Laboratory, Idaho Falls, ID. <https://doi.org/10.2172/1173081>.
- Collin, B. P., 2014. "AGR-2 Irradiation Test Final As-Run Report." INL/EXT-14-32277, Idaho National Laboratory, Idaho Falls, ID. <https://doi.org/10.2172/1514716>.
- Collin, B. P., 2016. "AGR-3/4 Irradiation Test Final As-Run Report." INL/EXT-15-35550, Idaho National Laboratory, Idaho Falls, ID. <https://doi.org/10.2172/1468992>.
- Demkowicz, P., L. Cole, S. Ploger, P. Winston, 2011. "AGR-1 Irradiated Test Train Preliminary Inspection and Disassembly First Look." INL/EXT-10-20722, Idaho National Laboratory, Idaho Falls, ID. <https://doi.org/10.2172/1009153>.
- Goeddel, V. W., G. R. Tully, R. A. Meyer, 1963. "The Use of Graphite in High-Temperature Nuclear Fuel Elements," In proceedings of the Fifth Conference on Carbon 2: 347-377.
<https://doi.org/10.1016/B978-0-08-009708-4.50034-1>.
- Entegris. 2013. "Graphite Properties and Characteristics." Entegris, Billerica, MA.
<https://poco.entegris.com/content/dam/poco/resources/reference-materials/brochures/brochure-graphite-properties-and-characteristics-11043.pdf>.
- Hawkes, G. L. 2014a. "AGR-1 Daily As-run Thermal Analyses." ECAR-968, Rev. 4. Idaho National Laboratory, Idaho Falls, ID.
- Hawkes, G. L. 2014b. "AGR-2 Daily As-Run Thermal Analysis" ECAR-2476, Rev. 0. Idaho National Laboratory, Idaho Falls, ID.
- Hawkes, G. L. 2015. "AGR-3/4 Daily As-Run Thermal Analyses." ECAR-2807, Rev. 0. Idaho National Laboratory, Idaho Falls, ID.
- Hawkes, G. L. 2022. "AGR-5/6/7 Daily As-Run Thermal Analyses." ECAR-5633, Idaho National Laboratory, Idaho Falls, ID.
- Hull, L., 2012. "NDMAS System and Process Description." INL/EXT-12-27594, Idaho National Laboratory, Idaho Falls, ID.
- Hunn, J. D., F. C. Montgomery, and P. J. Pappano. 2006a. "Data Compilation for AGR-1 Baseline Compact Lot LEU01-46T-Z." ORNL/TM-2006/507, Rev. 0. Oak Ridge National Laboratory, Oak Ridge, TN. <https://doi.org/10.2172/974600>.
- Hunn, J. D., and R. A. Lowden. 2006a. "Data Compilation for AGR-1 Baseline Coated Particle Composite LEU01-46T." ORNL/TM-2006/019, Rev. 1. Oak Ridge National Laboratory, Oak Ridge, TN. <https://doi.org/10.2172/974594>.
- Hunn, J. D., and R. A. Lowden. 2006b. "Data Compilation for AGR-1 Variant 1 Coated Particle Composite LEU01-47T." ORNL/TM-2006/020, Rev. 1. Oak Ridge National Laboratory, Oak Ridge, TN. <https://doi.org/10.2172/974595>.
- Hunn, J. D., F. C. Montgomery and P. J. Pappano. 2006b. "Data Compilation for AGR-1 Variant 1 Compact Lot LEU01-47T-Z." ORNL/TM-2006/508, Rev. 0. Oak Ridge National Laboratory, Oak Ridge, TN. <https://doi.org/10.2172/974601>.

- Hunn, J. D., and R. A. Lowden. 2006c. "Data Compilation for AGR-1 Variant 2 Coated Particle Composite LEU01-48T." ORNL/TM-2006/021, Rev. 1. Oak Ridge National Laboratory, Oak Ridge, TN. <https://info.ornl.gov/sites/publications/files/Pub1859.pdf>.
- Hunn, J. D., F. C. Montgomery, and P. J. Pappano. 2006c. "Data Compilation for AGR-1 Variant 2 Compact Lot LEU01-48T-Z." ORNL/TM-2006/509, Rev. 0. Oak Ridge National Laboratory, Oak Ridge, TN. <https://doi.org/10.2172/974602>.
- Hunn, J. D., and R. A. Lowden. 2006d. "Data Compilation for AGR-1 Variant 3 Coated Particle Composite LEU01-49T." ORNL/TM-2006/022, Rev. 0. Oak Ridge National Laboratory, Oak Ridge, TN. <https://info.ornl.gov/sites/publications/Files/Pub1860.pdf>.
- Hunn, J. D., F.C. Montgomery, and P.J. Pappano. 2006d. "Data Compilation for AGR-1 Variant 3 Compact Lot LEU01-49T-Z." ORNL/TM-2006/510, Rev. 0. Oak Ridge National Laboratory, Oak Ridge, TN. <https://info.ornl.gov/sites/publications/files/Pub2170.pdf>.
- Hunn, J. D., F.C. Montgomery, and P.J. Pappano. 2006e. "Data Compilation for AGR-2 B&W UO2 Compact Lot LEU11-OP2-Z." ORNL/TM-2010/055, Rev. 1 Oak Ridge National Laboratory, Oak Ridge, TN. <https://info.ornl.gov/sites/publications/Files/Pub139745.pdf>.
- Hunn, J. D., F.C. Montgomery, and P.J. Pappano. 2006f. "Data Compilation for AGR-2 UCO Variant Compact Lot LEU09-OP2-Z." ORNL/TM-2010/017, Rev. 1 Oak Ridge National Laboratory, Oak Ridge, TN. <https://info.ornl.gov/sites/publications/Files/Pub139744.pdf>.
- Hunn, J. D., F.C. Montgomery, and P.J. Pappano. 2006g. "Data Compilation for AGR-2 PBMR UO2 Compact Lot LEU08-OP3-Z." ORNL/TM-2010/070, Rev 0. Oak Ridge National Laboratory, Oak Ridge, TN.
- Hunn, J. D. 2007. "Data Compilation for AGR-3/4 Driver Fuel Coated Particle Composite LEU03-09T." ORNL/TM-2007/019, Rev. 0. Oak Ridge National Laboratory, Oak Ridge, TN.
- Hunn, J. D. 2011. "Data Compilation for AGR-3/4 Designed-to-Fail (DTF) Fuel Compact Lot (LEU03-10TOP2/LEU03-07DTF-OP1)-Z." ORNL/TM-2011/124, Rev. 0. Oak Ridge National Laboratory, Oak Ridge, TN.
- Kercher, A. K., et al. 2011. "Data Compilation for AGR-3/4 Designed-To-Fail (DTF) Fuel Particle Batch LEU03-07DTF." ORNL/TM-2011/109, Rev. 0. Oak Ridge National Laboratory, Oak Ridge, TN. <https://doi.org/10.2172/1649083>.
- Marsden, B. J., M. Haverty, W. Bodel, G. N. Hall, A. N. Jones, P. M. Mummery, and M. Treifi. 2016. "Dimensional change, irradiation creep and thermal/mechanical property changes in nuclear graphite." *International Materials Reviews* 61(3): 155-182. <https://doi.org/10.1080/09506608.2015.1136460>.
- Marshall D.W. 2019. "AGR-5/6/7 Fuel Fabrication Report." INL/EXT-19-53720, Rev. 0. Idaho National Laboratory, <https://doi.org/10.2172/1512795>.
- Petti, D. A., P.A. Demkowicz, J.T. Maki, and R.R. Hobbins. 2012. "TRISO-Coated Particle Fuel Performance." *Comprehensive Nuclear Materials* 3: 151-213. <https://doi.org/10.1016/B978-0-08-056033-5.00055-0>.
- Pham, B. T., J. J. Palmer, D. W. Marshall, J. W. Sterbentz, G. L. Hawkes, and D. M. Scates. 2021. "AGR-5/6/7 Irradiation Test Final As-Run Report." INL/EXT-21-64221. Idaho National Laboratory, Idaho Falls, ID. <https://www.osti.gov/biblio/1822435>.
- Ploger, S., P. Demkowicz, and J. Harp. 2015. "AGR-2 Irradiated Test Train Preliminary Inspection and Disassembly First Look." INL/EXT-15-34997, Idaho National Laboratory, Idaho Falls, ID. <https://doi.org/10.2172/1194020>.

- R Core Team. 2023. “R: A language and environment for statistical computing.” Vienna, Austria. URL <https://www.R-project.org/>.
- SAS Institute Inc. 2013. “SAS/ACCESS® 9.4 Interface to ADABAS: Reference.” SAS Institute Inc., Cary, NC. <https://documentation.sas.com/api/docsets/acadbas/9.4/content/acadbas.pdf?locale=en>.
- Stempien, J., F. J. Rice, P. L. Winston, and J. M. Harp. 2016. “AGR-3/4 Irradiation Test Train Disassembly and Component Metrology First Look Report.” INL/EXT-16-38005, Idaho National Laboratory, Idaho Falls, ID. <https://doi.org/10.2172/1364232>.
- Stempien, J. D., and L. Cai. 2023. “AGR-5/6/7 Irradiation Disassembly and Metrology First Look.” INL/RPT-23-71033, Rev 0. Idaho National Laboratory, Idaho Falls, ID. <https://doi.org/10.2172/1960206>.
- Sterbentz, J. W. 2013. “JMOCUP as-Run Daily Depletion Calculation for the AGR-1 Experiment in ATR B-10 Position.” ECAR-958, Rev. 2. Idaho National Laboratory, Idaho Falls, ID.
- Sterbentz, J. W. 2015a. “JMOCUP as-run Daily Depletion Calculation for the AGR-2 Experiment in ATR B-12 Position.” ECAR-2066, Rev. 2. Idaho National Laboratory, Idaho Falls, ID.
- Sterbentz, J. W. 2015b. “JMOCUP as-run Daily Physics Depletion Calculation for the AGR-3/4 TRISO Particle Experiment in ATR Northeast Flux Trap.” ECAR-2753, Rev. 1. Idaho National Laboratory, Idaho Falls, ID.
- Sterbentz, J. W. 2020. “JMOCUP Physics Depletion Calculations for the As-Run AGR-5/6/7 TRISO Particle Experiment in ATR Northeast Flux Trap.” INL/MIS-20-60700, Idaho National Laboratory, Idaho Falls, ID. <https://www.osti.gov/biblio/1774808>.
- Wickham, A. J. 2014. “Treatment Options for the Disposal Of Radioactive Graphite Wastes.” https://www.iaea.org/NuclearPower/Downloadable/Meetings/2015/2015-02-25-02-27-NPTDS/Day2/B04-Treatment_Options_for_i-Graphite.pdf. [Accessed 23 December 2015].
- Windes, W. E., P. L. Winston, and W.D. Swank. 2014. “AGC-2 Disassembly Report.” INL/EXT-14-32060, Idaho National Laboratory, Idaho Falls, ID. <https://doi.org/10.2172/1164855>.
- Windes, W. E., W. D. Swank, D. T. Rohrbaugh, and D. L. Cottle. 2015. “AGC-2 Specimen Post-Irradiation Data Package Report.” INL/EXT-15-36244, Idaho National Laboratory, Idaho Falls, ID. <https://doi.org/10.2172/1260881>.
- White, H. 1980. “A Heteroskedasticity-Consistent Covariance Matrix Estimator and a Direct Test for Heteroskedasticity.” *Econometrica* 48(4): 817–838. <https://doi.org/10.2307/1912934>.